© 2017. Published by The Company of Biologists Ltd | Development (2017) 144, 1674-1686 doi:10.1242/dev.147504

RESEARCH ARTICLE

Inhibition of ectopic microtubule assembly by the kinesin-13 KLP-7 prevents chromosome segregation and cytokinesis defects in oocytes

Emmanuelle Gigant[1,*], Marine Stefanutti[1,*], Kimberley Laband[1], Agata Gluszek-Kustusz[2], Frances Edwards[1], Benjamin Lacroix[1], Gilliane Maton[1], Julie C. Canman[3], Julie P. I. Welburn[2] and Julien Dumont[1,‡]

ABSTRACT

In most species, oocytes lack centrosomes. Accurate meiotic spindle assembly and chromosome segregation – essential to prevent miscarriage or developmental defects – thus occur through atypical mechanisms that are not well characterized. Using quantitative *in vitro* and *in vivo* functional assays in the *C. elegans* oocyte, we provide novel evidence that the kinesin-13 KLP-7 promotes destabilization of the whole cellular microtubule network. By counteracting ectopic microtubule assembly and disorganization of the microtubule network, this function is strictly required for spindle organization, chromosome segregation and cytokinesis in meiotic cells. Strikingly, when centrosome activity was experimentally reduced, the absence of KLP-7 or the mammalian kinesin-13 protein MCAK (KIF2C) also resulted in ectopic microtubule asters during mitosis in *C. elegans* zygotes or HeLa cells, respectively. Our results highlight the general function of kinesin-13 microtubule depolymerases in preventing ectopic, spontaneous microtubule assembly when centrosome activity is defective or absent, which would otherwise lead to spindle microtubule disorganization and aneuploidy.

KEY WORDS: Cytoskeleton, Microtubule dynamics, Meiotic spindle, Chromosome segregation, Microtubule depolymerase, Polar body extrusion

INTRODUCTION

Sexual reproduction relies on meiosis, a specialized type of cell division, which generates haploid germ cells or gametes. The genome size reduction that occurs during gametogenesis involves two successive cell divisions, termed meiosis I and II, preceded by a single round of genome replication (Dumont and Brunet, 2010). Chromosome gain or loss during meiosis generates aneuploid embryos after fertilization. Aneuploidy is hence a major obstacle in achieving reproductive success, as the vast majority of embryos formed from aneuploid oocytes are non-viable, leading to miscarriage (Nagaoka et al., 2012).

Accurate chromosome segregation is driven by the microtubule-based spindle. In somatic cells and spermatocytes, spindle microtubules are primarily assembled from the centrosomes, which duplicate once per cell cycle to form the two spindle poles (Walczak and Heald, 2008; Heald and Khodjakov, 2015). Chromosome alignment on the spindle and segregation in anaphase then occur through the interaction between spindle microtubules and kinetochores (Cheeseman, 2014). Chromosome spatial segregation is followed by their definitive physical separation during cytokinesis of the newly formed daughter cells (Green et al., 2012).

The generation of oocytes involves three major adaptations to the classical mechanism of cell division (Ohkura, 2015). First oocytes of most species lack conventional centriole-containing centrosomes (Szollosi et al., 1972). Spindle assembly in oocytes involves specific mechanisms such as chromatin-dependent microtubule assembly (Heald et al., 1996; Dumont and Desai, 2012). The second important adaptation of the meiotic cell division process, as yet only observed in *C. elegans* oocytes, is kinetochore-independent chromosome segregation (Dumont et al., 2010). The precise mechanism of this atypical segregation is still unclear but involves microtubule-dependent forces exerted on chromosomes (Dumont et al., 2010; Muscat et al., 2015; McNally et al., 2016). The third specific adaptation of oocyte meiosis is polar body extrusion (PBE), which corresponds to an extremely asymmetric partitioning of the oocyte creating a tiny polar body with most of the cytoplasm maintained in the oocyte (Zhang et al., 2008; Dorn et al., 2010; Fabritius et al., 2011; Maddox et al., 2012).

All three of these major adaptations to cell division essential for successful oocyte meiosis involve microtubules. Consequently, spindle microtubule dynamics in oocytes must be tightly regulated both temporally and spatially to successfully execute the meiotic cell division program. This is achieved primarily through the combined activities of microtubule-associated proteins (MAPs) and microtubule motors (Alfaro-Aco and Petry, 2015). Crucial among these are the microtubule-depolymerizing kinesin-13 family members (Walczak et al., 2013). Kinesin-13 proteins use the energy from ATP hydrolysis to depolymerize microtubules, and play essential roles in spindle assembly and chromosome segregation during mitosis (Wordeman and Mitchison, 1995; Walczak et al., 1996; Desai et al., 1999). Human mitotic cells depleted of the kinesin-13 MCAK (KIF2C) assemble spindles with abnormally long and stable microtubules that correlate with a high frequency of chromosome misattachments (Maney et al., 1998; Kline-Smith et al., 2004; Rogers et al., 2004; Domnitz et al., 2012). In mitotic *C. elegans* embryos, the unique kinesin-13 family member KLP-7 prevents assembly of an abnormally high number of astral microtubules and thus protects against an excessive increase in astral cortical pulling forces (Srayko et al., 2005). Accordingly, in KLP-7-depleted embryos the mitotic spindles break apart during

[1]Institut Jacques Monod, CNRS, UMR 7592, University Paris Diderot, Sorbonne Paris Cité, Paris F-75205, France. [2]Wellcome Trust Centre for Cell Biology, School of Biological Sciences, University of Edinburgh, Edinburgh EH9 3JR, Scotland, UK. [3]Columbia University, Department of Pathology and Cell Biology, New York, NY 10032, USA.
*These authors contributed equally to this work

‡Author for correspondence (julien.dumont@ijm.fr)

E.G., 0000-0001-9098-0994; J.D., 0000-0001-5312-9770

Received 25 November 2016; Accepted 7 March 2017

Development (2017) 144, 1674-1686 doi:10.1242/dev.147504

anaphase and sister chromatids separate prematurely (Grill et al., 2001).

During oocyte meiosis kinesin-13 proteins are involved in multiple aspects of cell division, including the control of meiotic spindle length and proper chromosome alignment (Zou et al., 2008; Illingworth et al., 2010; Radford et al., 2012; Do et al., 2014). In the *C. elegans* oocyte, KLP-7 has been proposed to limit metaphase spindle pole numbers by correcting improper kinetochore-microtubule attachments, but its precise function throughout the two meiotic divisions remains elusive (Connolly et al., 2015; Han et al., 2015). Here, we show the crucial meiotic function of KLP-7 in preventing ectopic microtubule assembly that otherwise leads to spindle disorganization and chromosome segregation defects. We provide the first high-resolution, time-resolved comprehensive view of meiotic divisions in the *C. elegans* oocyte. Specifically, we show that KLP-7 acts by globally destabilizing microtubules within the meiotic spindle in metaphase and the central spindle in anaphase, as well as throughout the oocyte cell cortex. We also demonstrate that KLP-7 or MCAK activities prevent ectopic cytoplasmic aster formation during mitosis in the *C. elegans* zygote or in HeLa cells, respectively, when centrosome function is impaired. Our data suggest that the function of kinesin-13 is essential to delimit the proper local assembly of microtubules in dividing cells when centrosome activity is reduced or absent, and thus for accurate spindle assembly.

RESULTS

In utero imaging reveals that KLP-7 is required for the initial step of meiotic spindle assembly and bipolarization

We sought to test the role of KLP-7 during meiotic spindle assembly. We first verified that our RNAi-mediated depletion strategy led to a strong embryonic lethality phenotype comparable to the *klp-7* deletion mutant (hereafter *klp-7Δ*), and completely removed KLP-7 from oocytes (Fig. S1A,B). We also verified that expressing a functional GFP-tagged RNAi-resistant KLP-7 protein rescued this embryonic lethality (Fig. S1C,D). We then analyzed nuclear envelope breakdown (NEBD) and meiotic spindle assembly in control and KLP-7-depleted oocytes during both meiotic divisions *in utero* in immobilized worms expressing GFP-tagged β-tubulin or the microtubule minus-end and spindle pole marker protein Abnormal spindle protein 1 (ASPM-1) and mCherry-tagged histone 2B (H2B) (van der Voet et al., 2009). Spindle assembly can be separated into four distinct phases (Wolff et al., 2016). In both control and KLP-7-depleted oocytes before NEBD, microtubules were excluded from the nucleus (Fig. 1A,B, Fig. S2A,B). In controls, after NEBD (evidenced by the diffusion of the soluble pool of fluorescent H2B away from the nucleoplasm), microtubules progressively invaded the nucleus to form a diffuse nuclear cloud around chromosomes (Fig. S2A,B, Movie 1). In KLP-7-depleted oocytes and consistent with the cytoplasmic localization of GFP::KLP-7 in control oocytes at this stage, more microtubules were visible around the nucleus before NEBD relative to controls (Fig. 1A, Fig. S2A,B, Movies 1 and 2). Strikingly, the first phase of spindle assembly never took place in KLP-7-depleted oocytes and the diffuse microtubule cloud that formed at NEBD around chromosomes in controls was completely absent (Fig. 1C,D). Instead, ectopic microtubules persisted after NEBD around the breaking nuclear envelope. KLP-7 is therefore essential for the formation of a microtubule cloud around chromosomes after NEBD.

During the second phase, GFP::KLP-7 progressively accumulated on chromosomes and the assembled diffuse network of microtubules became bundled and coalesced around chromosomes in control oocytes (Fig. 1A,B,E, Movie 2). In parallel, the chromosomes became clustered together. In controls, this second phase correlated with the appearance of ASPM-1 foci around chromosomes (Fig. 1F, Fig. S1C, Movie 3). Progressive microtubule bundling and cross-linking led to the formation of a multipolar spindle with several ASPM-1 foci around chromosomes (Connolly et al., 2015). GFP::KLP-7 also concentrated on these multiple poles (Fig. 1E). In controls, this phase was accompanied by the dispersal of chromosomes on the forming spindle and their subsequent congression and alignment. In KLP-7-depleted oocytes, the ectopic perinuclear microtubules seen in phase 1 coalesced around chromosomes during phase 2 to form a multipolar spindle that displayed multiple ASPM-1 foci as in controls (Fig. 1F, Fig. S2C, Movie 3). Thus, although the oocytes started phase 2 in the absence of a diffuse microtubule cloud around chromosomes and with ectopic perinuclear microtubules, KLP-7-depleted oocytes formed a seemingly normal multipolar spindle early in meiosis I.

During phase 3 in controls, the multipolar microtubule structure was slowly shaped into a bipolar spindle and ASPM-1 and GFP::KLP-7 concentrated at the spindle poles. In KLP-7-depleted oocytes, the multiple microtubule foci persisted and a bipolar spindle was almost never observed until after anaphase onset (see below). Similar imaging experiments in a strain expressing the nuclear envelope component Lamin 1 (LMN-1) tagged with GFP and mCherry-tagged β-tubulin revealed that the entire process of initial meiotic spindle assembly took place within the limits of the rupturing nuclear envelope (Fig. 1G, Fig. S1D, Movie 4). In both controls and KLP-7-depleted oocytes, nuclear envelope remnants were visible around the spindle up until the end of the bipolarization phase. KLP-7 therefore plays a crucial role in phase 3, and is required for bipolar spindle formation at this stage.

In controls, phase 4, as previously described, corresponded to an extensive spindle pole disassembly (Yang et al., 2003). KLP-7-depleted oocytes did not usually reach bipolar spindle assembly, but *klp-7(RNAi)* did not affect the overall timing of nuclear envelope disassembly or anaphase onset (Fig. 1B,G, Fig. S1D, Movie 4). After anaphase onset, spindle bipolarity in KLP-7-depleted oocytes was almost always rescued, due largely to 'polar clustering'. Thus, although disruption of KLP-7 activity leads to multipolar spindle assembly prior to anaphase, spindle bipolarity appears to be established prior to or during meiotic anaphase and cytokinesis (see also below).

High-resolution *ex utero* imaging shows that KLP-7 is required for normal meiotic spindle microtubule organization and full chromosome segregation

To further investigate the contribution of KLP-7 to acentrosomal spindle assembly and function, we filmed *ex utero* fertilized oocytes expressing GFP-tagged β-tubulin and mCherry-tagged H2B, which allows for higher spatial resolution (Fig. 2A, Movie 5). Control oocytes had all completed meiosis I spindle bipolarization at the time of dissection. In KLP-7-depleted or -deleted oocytes, spindle microtubule density (measured by average GFP::β-tubulin intensity) was increased as compared with controls at every step of meiosis I and II (Fig. 2B, Movie 5). In controls, the barrel-shaped meiosis I spindle displayed a few extremely short microtubules extending outward (Fig. 2C). By contrast, KLP-7-depleted oocytes displayed disorganized spindles with numerous long microtubules or microtubule bundles extending out toward the cytoplasm and the oocyte cortex (Fig. 2C). In agreement with a previous study and with our *in utero* analysis, we found that spindles assembled in KLP-7-depleted oocytes were multipolar (Connolly et al., 2015)

Development (2017) 144, 1674-1686 doi:10.1242/dev.147504

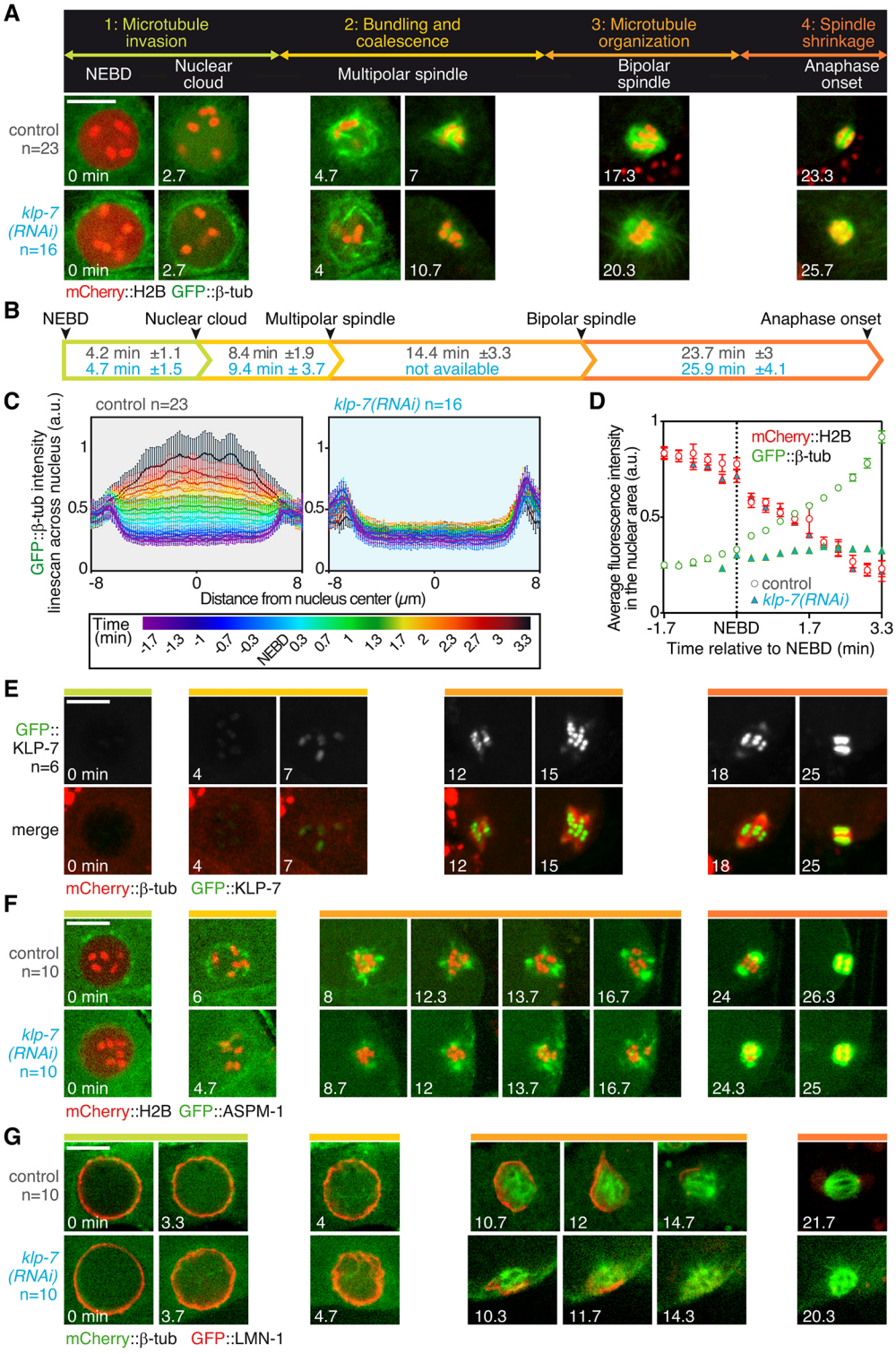

Fig. 1. KLP-7 is required for meiotic spindle assembly. (A) Still images from *in vivo* live imaging of oocytes expressing GFP-tagged β-tubulin and mCherry-tagged H2B showing the four phases of meiosis I spindle assembly in the indicated conditions. Timings are relative to NEBD. (B) Average timings relative to NEBD of the four phases of spindle assembly in control and KLP-7-depleted oocytes. (C) Fluorescence intensity line scan of GFP-tagged β-tubulin across the nucleus between 1.7 min before NEBD and 3.3 min after NEBD (timings are color-coded according to the horizontal scale presented at the bottom). 0 μm corresponds to the center of the nucleus. The sample size (number of oocytes analyzed) is indicated and was generated by aggregation over six independent experiments. Error bars represent s.e.m. (D) Average fluorescence intensity of GFP-tagged β-tubulin and mCherry-tagged H2B in the nuclear area between 1.7 min before NEBD and 3.3 min after NEBD. Error bars represent s.d. (E) Still images from *in vivo* live imaging in oocytes expressing GFP-tagged KLP-7 and mCherry-tagged β-tubulin. (F) Still images from *in vivo* live imaging in oocytes expressing GFP-tagged ASPM-1 and mCherry-tagged H2B showing the four phases (indicated by the color-coded line above each image) of meiosis I spindle assembly in the indicated conditions. Timings are relative to NEBD. (G) Still images from *in vivo* live imaging in oocytes expressing GFP-tagged LMN-1 and mCherry-tagged H2B showing the four phases of meiosis I spindle assembly in the indicated conditions. Scale bars: 10 μm.

(Fig. 2D). However, we found that the supernumerary poles were always resolved and incorporated into one of the two dominant spindle poles at or just after anaphase onset.

We next monitored the progression and accuracy of meiotic chromosome segregation in the presence and absence of KLP-7 in embryos (Fig. 2E). The overall timing of divisions was not significantly different between control and KLP-7-depleted or -deleted oocytes (Fig. 2H). In control oocytes, chromosomes aligned on tight metaphase plates during metaphase I and II. Segregating chromosomes remained tightly clustered during both anaphase I and II, which usually ended with successful PBE. By contrast and consistent with the spindle disorganization that we described above, KLP-7 depletion or deletion led to visible chromosome alignment and segregation defects during both meiotic divisions (Fig. 2E). Chromosome masses always separated after anaphase onset and lagging chromosomes were evident in most oocytes. Chromosome counting in fixed meiosis II oocytes that succeeded in first PBE revealed significant aneuploidy

Development (2017) 144, 1674-1686 doi:10.1242/dev.147504

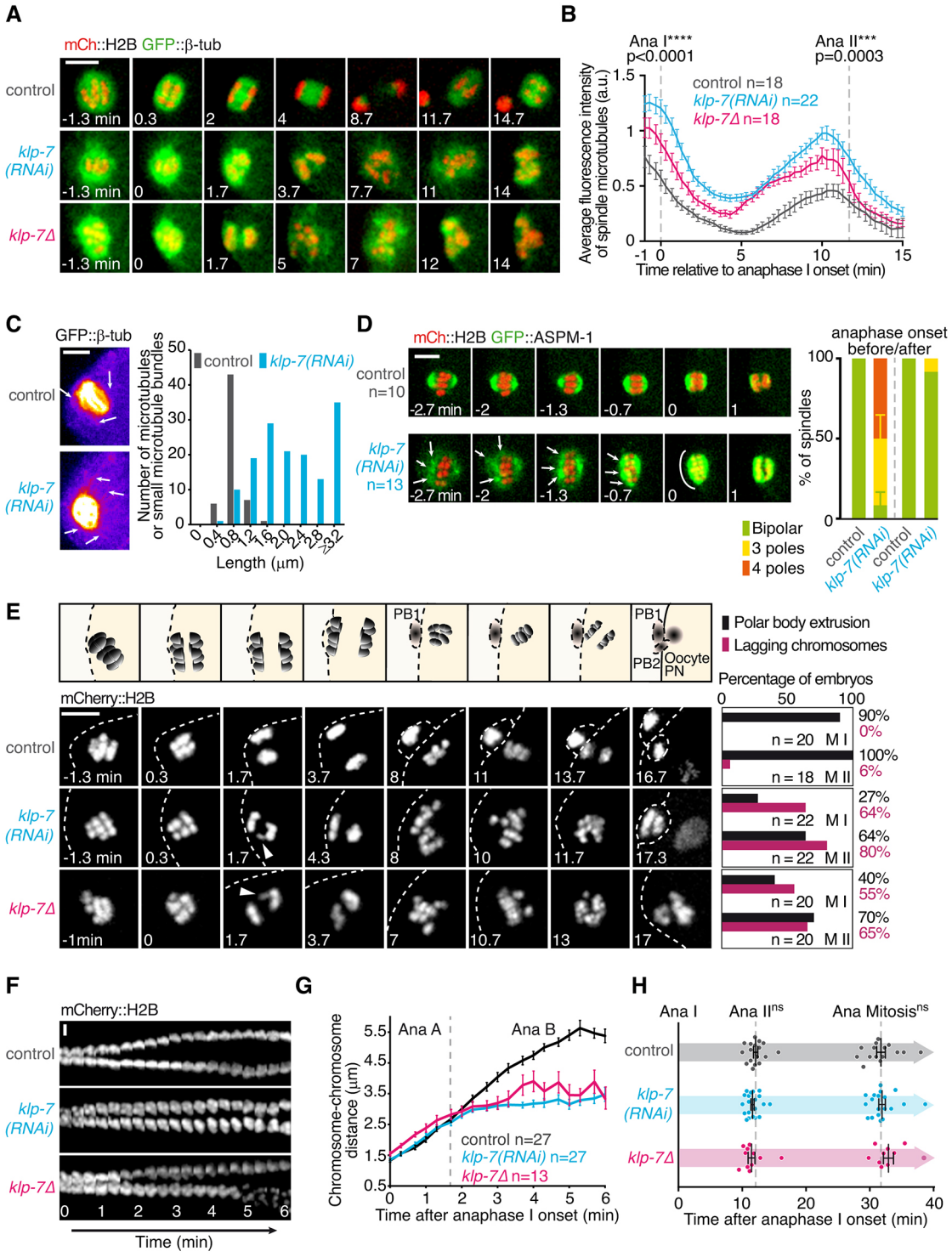

Fig. 2. See next page for legend.

(control, 6 chromosomes in 14/14 oocytes; *klp-7(RNAi)*, 4 chromosomes in 2/15 oocytes, 5 in 5/15, 6 in 7/15 and 7 in 1/15; *klp-7Δ*, 4 chromosomes in 2/16 oocytes, 5 in 6/16, 6 in 6/16 and 7 in 2/16). As expected, KLP-7 depletion or deletion did not affect chromosome number during meiosis I (control, 6 chromosomes in 24/24 oocytes; *klp-7(RNAi)*, 6 chromosomes in 20/20 oocytes; *klp-7Δ*, 6 chromosomes in 20/20 oocytes).

We also found that KLP-7 is required for full chromosome segregation in meiosis I. Kymographs of anaphase I revealed that chromosome masses in KLP-7-depleted or -deleted oocytes separated at a rate comparable to controls during the first 2 min following anaphase onset (Fig. 2F,G). This timing corresponds approximately to the duration of anaphase A during meiosis I in *C. elegans* oocytes (McNally et al., 2016). Chromosomes in controls continued to separate during anaphase B for the following 3 min and reached a maximal distance of 5.5 µm. In striking contrast, chromosome masses abruptly slowed down in KLP-7-depleted or -deleted oocytes 1.5 min after anaphase onset and chromosome separation paused at a distance of

Development (2017) 144, 1674-1686 doi:10.1242/dev.147504

Fig. 2. KLP-7 promotes proper meiotic spindle organization and chromosome segregation. (A) Still images from live imaging in oocytes expressing GFP-tagged β-tubulin and mCherry-tagged H2B between prometaphase I and anaphase II. Timings are relative to anaphase I onset. (B) Quantification of the spindle microtubule average intensity over time in the indicated conditions. Error bars represent s.e.m. (C) Pseudocolored still images of metaphase I spindles in control and KLP-7-depleted oocytes (left). Arrows indicate microtubules or microtubule bundles emanating from the meiotic spindle. Distribution of the length of microtubules or microtubule bundles emanating from meiosis I spindles in control and KLP-7-depleted oocytes (right). (D) Still images from *in vivo* live imaging in oocytes expressing GFP-tagged ASPM-1 and mCherry-tagged H2B, highlighting the dynamics of spindle poles during anaphase I. Timings are relative to anaphase I onset (left). Arrows indicate microtubules or microtubule bundles emanating from the meiotic spindle. Quantification of the spindle pole number in control and KLP-7-depleted oocytes before (−20 s) and after (+20 s) anaphase onset (right). (E) Top row shows a schematic representation of chromosome segregation during meiosis I and II. PB1, first polar body; PB2, second polar body; PN, pronucleus. Dashed lines indicate the oocyte contour. Bottom rows are still images from live imaging of mCherry-tagged H2B-expressing fertilized oocytes. Timings are relative to anaphase I onset. In the KLP-7 depletion and deletion images, the arrowheads indicate lagging chromosomes during anaphase I. Quantification of lagging chromosomes during anaphase I and II and of polar body extrusion (MI, meiosis I; MII, meiosis II) is shown on the right. (F) Kymographs, initiated at anaphase I onset, showing movements of chromosomes during anaphase I. The time interval between consecutive strips is 20 s. (G) Quantification of separation between chromosome masses over time in control and KLP-7-depleted or -deleted oocytes. Error bars represent s.e.m. (H) The timing of meiotic divisions and of the first embryonic mitosis is not affected by depletion or deletion of KLP-7. Error bars represent s.e.m. Unpaired *t*-tests with Welch's correction were used to determine significance. Ana I-II: control versus *klp-7(RNAi)* P=0.2426; control versus *klp-7Δ* P=0.2081. Ana I-Mitosis: control versus *klp-7(RNAi)* P=0.8367; control versus *klp-7Δ* P=0.3315. Scale bars: 5 µm in A,C-E; 2 µm in F.

~2.5 µm (Fig. 2G). Abnormal chromosome segregation was frequently followed by unsuccessful PBE and the formation of a multi-pronucleate polyploid embryo (Fig. 2E). KLP-7 is therefore essential for anaphase B chromosome movements and for the overall accuracy and success of meiotic chromosome segregation.

KLP-7 promotes meiotic central spindle assembly and PBE

The defects that we observed in chromosome segregation and PBE in KLP-7-depleted or -deleted oocytes prompted us to analyze anaphase I central spindle organization and function, this spindle being essential for both chromosome segregation and PBE in the *C. elegans* oocyte (Dumont et al., 2010; Fabritius et al., 2011). Deconvolution microscopy on fixed oocytes in anaphase I showed obvious central spindle microtubule organization defects in KLP-7-depleted oocytes (Fig. 3A).

To understand KLP-7 function in meiotic central spindle assembly and in polar body cytokinesis, we analyzed microtubule organization and density over time by live imaging during anaphase I. We filmed oocytes expressing GFP-tagged β-tubulin and mCherry-tagged H2B (Fig. 3B, Fig. S3A). We noticed that the microtubule structures were more dense during anaphase in KLP-7-depleted oocytes. Specifically, the segregating chromosome masses were devoid of microtubules in controls but remained embedded in a microtubule mesh throughout anaphase in KLP-7-depleted oocytes. Consistent with this, the microtubule minus-end marker ASPM-1 was abnormally concentrated around the segregating chromosomes throughout anaphase (Fig. 3C, Table S1). Thus, ectopic microtubules assembled in the vicinity of chromosomes persisted throughout anaphase in KLP-7-depleted oocytes leading to central spindle defects.

To test whether these defects directly affect central spindle component localization, we analyzed the dynamic recruitment of the central spindle microtubule bundling protein SPD-1 (ortholog of PRC1) and of the Centralspindlin complex subunit CYK-4 (ortholog of MgcRacGAP or RACGAP1). Both proteins are normally specifically recruited on central spindle microtubules during anaphase, where they are essential for microtubule organization and cytokinesis (Mishima et al., 2002; Verbrugghe and White, 2004; Glotzer, 2005; Maton et al., 2015). The dense and disorganized microtubules of the central spindle in KLP-7-depleted oocytes correlated with a reduction in the recruitment of these two proteins to the meiotic central spindle and with ectopic CYK-4 on chromosomes (Fig. 3D,E, Movie 6, Table S1). The lack of KLP-7 therefore leads to the mislocalization of essential central spindle components, which is likely to contribute to the observed central spindle defects.

In control oocytes, recruitment of central spindle components ultimately leads to the formation of a contractile actomyosin ring that promotes plasma membrane furrowing and cytokinesis (Maddox et al., 2012). To test if the improper central spindle component localization in KLP-7-depleted oocytes correlated with defects in actomyosin organization, we analyzed oocytes expressing GFP-tagged myosin II (NMY-2) and mCherry-tagged H2B during anaphase I. Consistent with previous findings, in control oocytes NMY-2 formed a disc above the segregating chromosomes that progressively evolved into a cylinder, which ultimately formed the meiotic midbody between the segregated chromosomes (Dorn et al., 2010) (Fig. 3F, Movie 6, Table S1). In KLP-7-depleted oocytes, a normal disc of NMY-2 was initially visible above chromosomes but it strikingly almost never evolved into a cylinder. Instead, the set of chromosomes that would normally end up in the first polar body re-entered the oocyte cytoplasm and was surrounded by a thick layer of cortical NMY-2. Altogether, these results show that KLP-7 is essential for meiotic cytokinesis and PBE through its function in central spindle organization.

KLP-7 prevents the formation of ectopic cortical microtubule asters

A recent study analyzing feeding RNAi-mediated depletion of KLP-7 or a KLP-7 temperature-sensitive loss-of-function mutant showed that the multipolar spindle phenotype observed when KLP-7 activity is decreased could be rescued upon co-depletion of the NDC-80 kinetochore component (Connolly et al., 2015). That study concluded that KLP-7 is involved in destabilizing improper kinetochore-microtubule attachments established during early prometaphase, similar to the function of its vertebrate ortholog MCAK during mitosis. This in turn would release tension within meiotic spindles that would otherwise lead to extra spindle pole formation. Although we found a similar rescuing effect of the *ndc-80(RNAi)* on early prometaphase spindles assembled in *klp-7*-deleted oocytes, we noticed that these spindles were still disorganized during most of prometaphase/metaphase (Fig. S4A,B). Furthermore, depleting the core kinetochore scaffold protein KNL-1 did not rescue spindle bipolarity when KLP-7 is absent (Fig. S4A,B). Altogether, these results suggest that destabilizing kinetochore-microtubule attachments in oocytes is not sufficient to stably rescue bipolar spindle formation when KLP-7 is absent.

To understand the origin of the extra spindle poles that assemble in KLP-7-depleted or -deleted oocytes, we performed *ex utero* live imaging of the spindle assembly process in oocytes. In line with a previous study, we noticed the presence of numerous ectopic microtubule asters near the cell cortex of KLP-7-depleted or -deleted oocytes (Fig. 4A,B) (Han et al., 2015). Ectopic cortical asters persisted throughout meiosis but disappeared at anaphase II

Development (2017) 144, 1674-1686 doi:10.1242/dev.147504

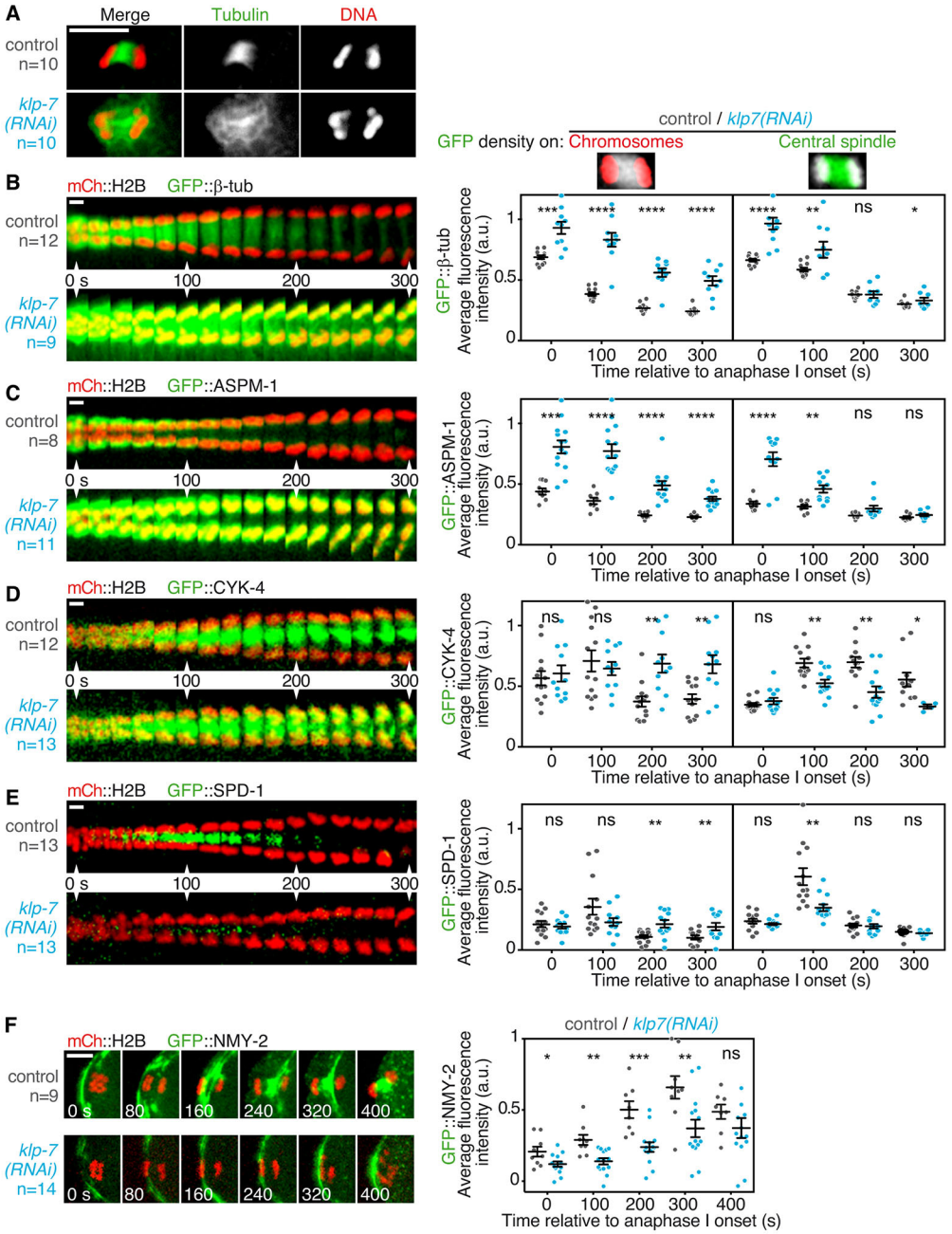

Fig. 3. KLP-7 promotes meiotic central spindle assembly and polar body extrusion. (A) KLP-7 depletion leads to central spindle microtubule disorganization during meiotic anaphase. (B-E) Montage of still images from live imaging experiments in GFP-tagged β-tubulin (B), GFP-tagged ASPM-1 (C), GFP-tagged CYK-4 (D), GFP-tagged SPD-1 (E) and mCherry-tagged H2B-expressing oocytes during anaphase I (left). The time interval between consecutive strips is 20 s. Quantifications of microtubule average intensity on chromosomes (red) or in the central spindle region (green) during anaphase are shown on the right. The quantified regions of interest are schematized in the top row. (F) Montage of still images from a live imaging experiment in oocytes expressing GFP-tagged NMY-2 and mCherry-tagged H2B during anaphase I (left). Timings are relative to anaphase I onset. Quantification of the GFP-tagged NMY-2 average intensity during anaphase I in a region of interest surrounding the chromosomes and the anaphase central spindle is shown on the right. *P*-values are indicated in Table S1. Error bars represent s.e.m. Scale bars: 5 µm in A,F; 2 µm in B-E.

onset (Fig. 4C). These asters displayed rapid movements at the cortex and tended to cluster together. Importantly, we observed a significant number of asters that aggregated at the metaphase spindle (Fig. 4D). Cortical asters were positive for ASPM-1, and when they were localized near the meiotic spindle they contributed to generating supernumerary spindle poles (Fig. 4E,F). Therefore, KLP-7 is required to prevent ectopic microtubule assembly at the cell cortex, which otherwise leads to the formation of extra spindle poles and contributes to the observed multipolar spindle phenotype.

KLP-7 is globally required for normal microtubule dynamics during meiosis

The longer and denser meiotic spindles and ectopic cortical microtubule asters observed suggested that microtubules are, overall, more stable after KLP-7 depletion. To test this hypothesis, we performed fluorescence recovery after photobleaching (FRAP) experiments of the entire metaphase I spindle in control and KLP-7-depleted oocytes that were genetically arrested in metaphase I (see Materials and Methods; Fig. 5A, Movie 7). Control metaphase I spindles were highly dynamic and recovered 86% of their initial fluorescence with a halftime of recovery ($t_{1/2}$) of 22.2 s. Meiotic spindles assembled in KLP-7-depleted oocytes also recovered almost completely (87% of initial fluorescence); however, recovery was delayed compared with controls with a $t_{1/2}$ of 33.3 s (Fig. 5B). Thus, although the proportion of fully stable spindle microtubules that did not recover fluorescence over the course of the quantification period was not significantly different (P=0.9765) in control or KLP-7-depleted oocytes, microtubules were on average more stable in the latter (P=0.0338).

To determine the origin and dynamics of the ectopic cortical microtubule asters, we performed spinning disc cortical live imaging in control and *klp-7*-deleted oocytes expressing GFP-

Development (2017) 144, 1674-1686 doi:10.1242/dev.147504

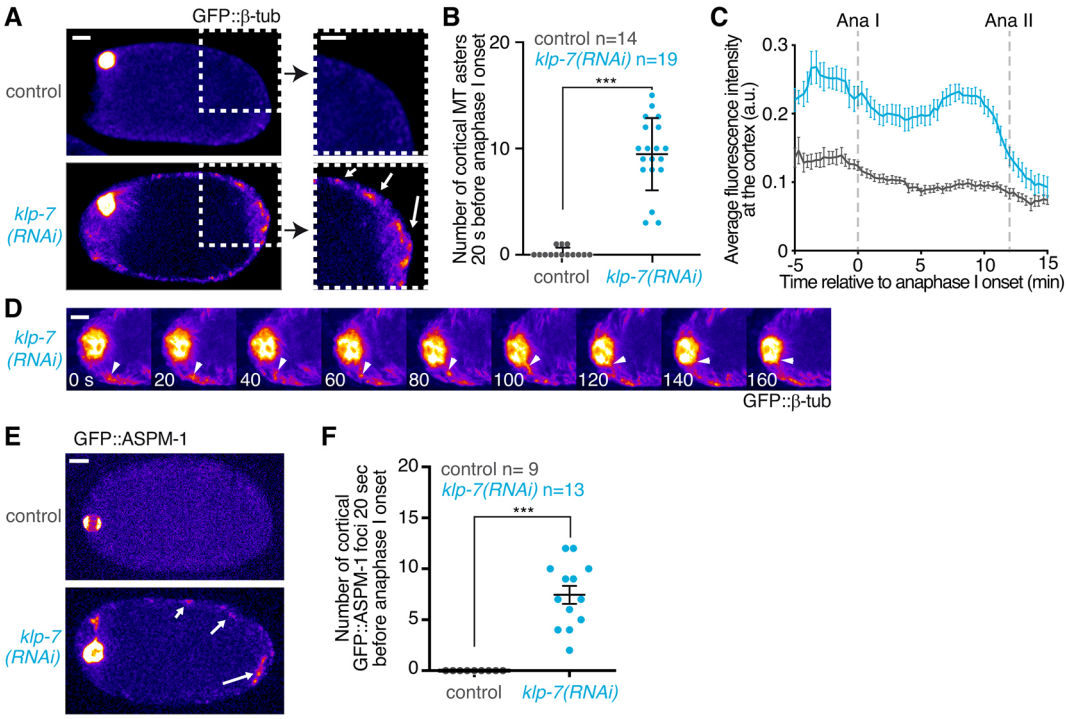

Fig. 4. KLP-7 prevents the formation of ectopic cortical microtubule asters that generate extra spindle poles. (A) Pseudocolored images from a live imaging experiment in GFP-tagged β-tubulin-expressing oocytes showing the ectopic cortical asters that form after KLP-7 depletion. Higher magnifications of a cortical region (dashed box) are shown on the right. Arrows in the KLP-7 image point to cortical asters. (B) Quantification of the cortical aster number 20 s before anaphase onset in control and KLP-7-depleted oocytes. Error bars represent s.e.m. Unpaired *t*-test with Welch's correction was used to determine significance (***P<0.0001). MT, microtubule. (C) Quantification of cortical average intensity of GFP::β-tubulin over time in the indicated conditions. Error bars represent s.e.m. (D) Pseudocolored still images from a live imaging experiment in GFP-tagged β-tubulin-expressing oocytes showing cortical aster movements and incorporation in the meiosis I spindle. Timings are relative to the first time point shown (0 s corresponds to prometaphase of meiosis I). Arrowhead indicates an ectopic microtubule aster moving and being incorporated in the meiotic spindle. (E) Pseudocolored images from a live imaging experiment in GFP-tagged ASPM-1-expressing oocytes showing the ectopic cortical asters that form after KLP-7 depletion. Arrows in the KLP-7 image point to cortical asters. (F) Quantification of the cortical aster number 20 s before anaphase onset in control and KLP-7-depleted oocytes. Error bars represent s.e.m. Unpaired *t*-test with Welch's correction was used to determine significance (***P<0.0001). Scale bars: 5 µm.

tagged β-tubulin (Fig. 5E,F). At the cell cortex, a dynamic cortical microtubule meshwork that slid rapidly in parallel with the cortex was visible in both control and *klp-7*-deleted oocytes (Fig. 5C-E). However, the microtubule meshwork was more dense in the absence of KLP-7, suggesting that global microtubule stabilization leads to the observed ectopic cortical microtubule asters (Fig. 5C). Consistent with this, cortical microtubules were overall less dynamic in *klp-7*-deleted oocytes, as evident by the increased time spent in pause (not growing or shrinking, $t_{control}$=28.1±29.4 s, $t_{klp\text{-}7\Delta}$=68.9±35.11 s, Fig. 5F) and the overall reduction of all microtubule dynamics parameters (Fig. 5G-I) (Lacroix et al., 2014). By applying a simple model of microtubule dynamics to our data, we calculated that the average theoretical length of microtubules in the absence of KLP-7 was higher than in control oocytes at steady state ($L_{control}$=6 µm, $L_{klp\text{-}7\Delta}$=8.2 µm; see Materials and Methods), which is consistent with our live observations (Verde et al., 1992). Thus, KLP-7 increases cortical microtubule dynamics in the *C. elegans* oocyte, preventing ectopic microtubule aster formation.

The kinesin-13 depolymerases KLP-7 and MCAK prevent ectopic microtubule assembly when centrosome activity is reduced or absent

Strikingly, the ectopic asters that formed in oocytes in the absence of KLP-7 were never observed in mitotic embryos. Instead, during mitosis, the absence of KLP-7 leads to increased astral microtubule density and a corresponding increase in astral microtubule pulling forces at centrosomes (Fig. S3B) (Srayko et al., 2005). To test if this difference between oocytes and zygotes could be linked to the presence of functional centrosomes in the zygote, we analyzed the effect of reducing centrosomal activity following depletion of the scaffold component SPD-5 in *klp-7*-deleted zygotes. In the absence of a functional centrosome in *spd-5(RNAi)* zygotes when KLP-7 is present, cytoplasmic asters were never observed and the few microtubules that assembled following NEBD always radiated from the condensed chromosomes (Fig. 6A) (Hamill et al., 2002). Strikingly, however, when SPD-5 was depleted in *klp-7*-deleted zygotes, numerous cytoplasmic ectopic asters assembled at NEBD at a distance from the chromosomes (Fig. 6A,B). These asters subsequently coalesced around the condensed chromosomes to form a single larger microtubule structure (not shown). Thus, in the absence of functional centrosomes in *C. elegans* zygotes, KLP-7 activity is essential to prevent ectopic microtubule assembly.

To test if this function of KLP-7 is a general feature of kinesin-13, we tested the effect of MCAK depletion in HeLa cells when centrosome activity is reduced during microtubule regrowth after nocodazole washout (Cavazza et al., 2016). Forty-five minutes after removing nocodazole, microtubules reassembled from two microtubule-organizing centers (MTOCs) on average in control cells (2.16±0.06; Fig. 6C,D). By contrast, three MTOCs (3.13±0.12) could be detected in most MCAK-depleted cells. Importantly, the effect of depleting MCAK was specific to cells in which centrosome activity was reduced by the nocodazole treatment. Thus,

Development (2017) 144, 1674-1686 doi:10.1242/dev.147504

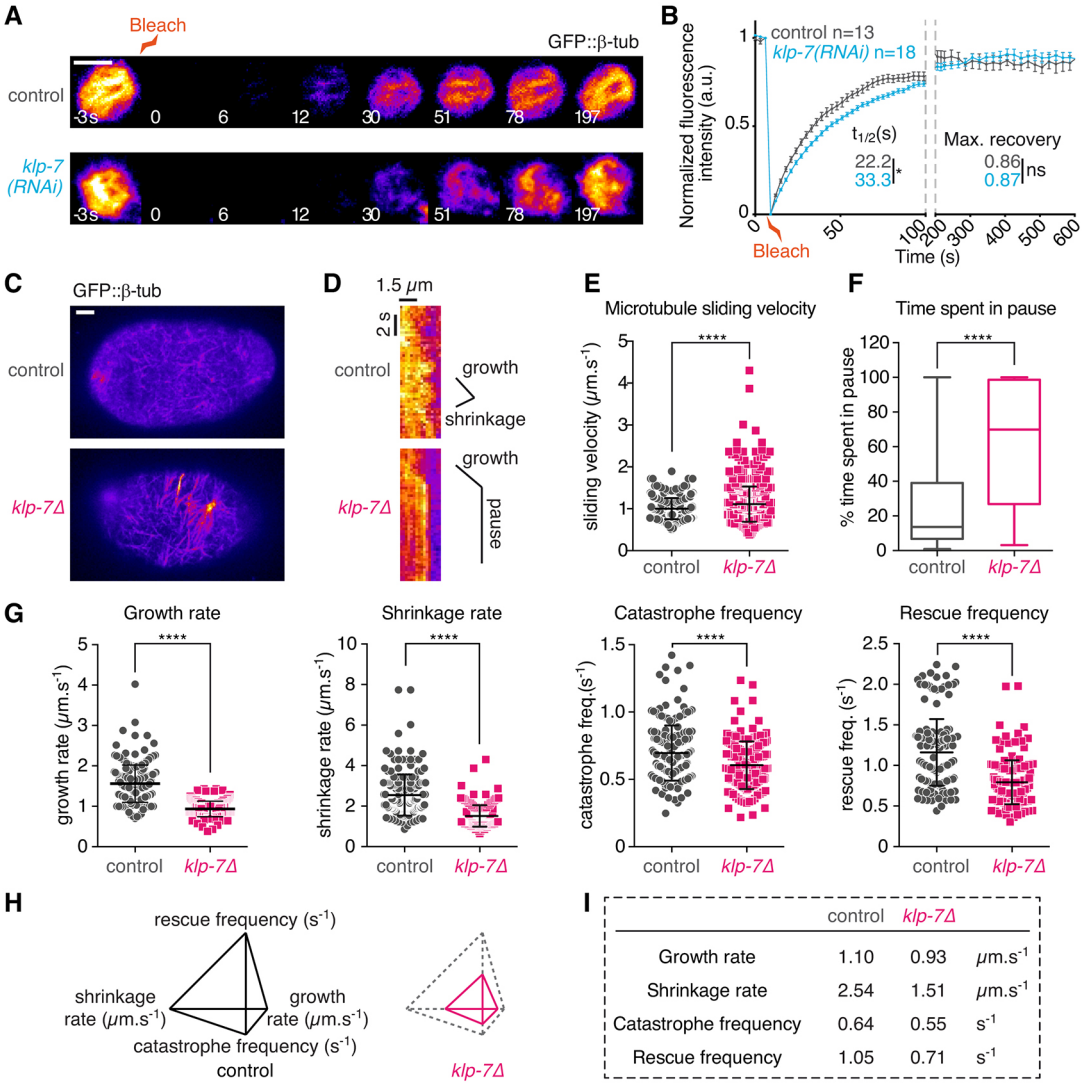

Fig. 5. KLP-7 is globally required for normal microtubule dynamics during oocyte meiosis. (A) Pseudocolored still images from a FRAP experiment in GFP-tagged β-tubulin-expressing oocytes artificially arrested in metaphase I. Timings are relative to the photobleaching event. Scale bar: 5 µm. (B) Quantification of the fluorescence recovery over time during the FRAP experiment. Error bars represent s.e.m. (C) Pseudocolored still images from a cortical live imaging experiment in GFP-tagged β-tubulin-expressing oocytes showing the dense microtubule meshwork present in *klp-7*-deleted oocytes. Scale bar: 5 µm. (D) Pseudocolored kymographs of individual cortical microtubules, showing their dynamics in control and *klp-7*-deleted oocytes. A schematic representation of a growth and shrinkage event in a control oocyte and of a growth and pause event in a *klp-7*-deleted oocyte is shown on the right. The time interval between consecutive strips is 250 ms. (E) Quantification of the microtubule sliding velocity in control and *klp-7*-deleted oocytes ($n \geq 210$ microtubules). Error bars represent s.d. (F) Quantification of the time spent in pause by individual microtubules in control and *klp-7*-deleted oocytes ($n \geq 130$ microtubules). Box plots represent the 75th percentile with the median indicated as a line and error bars represent s.d. (G) Quantification of the growth and shrinkage rates, catastrophe and rescue frequencies of individual microtubules in control and *klp-7*-deleted oocytes ($n \geq 160$ microtubules). Error bars represent s.d. (H) Diamond graph representing microtubule dynamics in control oocytes (left). Microtubule dynamics in control (dashed line) and *klp-7*-deleted (red) oocytes are compared using jointly normalized diamond graphs (right). (I) Average values for the four parameters used in the diamond graphs. Unpaired *t*-tests with Welch's correction were used throughout to determine significance (****$P<0.0001$ for all comparisons).

ectopic microtubule nucleation centers are activated in human cells with reduced centrosome activity when MCAK levels are decreased. Altogether, these results suggest that preventing ectopic microtubule assembly in cells with reduced or absent centrosome activity is a previously uncharacterized general and conserved function of kinesin-13 depolymerases (Fig. 6E).

DISCUSSION

KLP-7 is essential for the formation of a functional spindle in the *C. elegans* oocyte

Previous studies of meiotic spindle assembly in the *C. elegans* oocyte have been performed at relatively low spatial and temporal resolutions, did not provide temporal information and/or missed the very early steps of spindle assembly (Yang et al., 2003; Connolly et al., 2015; Wolff et al., 2016). Here, we provide a precise quantitative picture covering the full time window of interest and the first time-resolved analysis of the entire process of meiotic spindle formation in this system. Oocytes of most species lack centriole-containing centrosomes, and microtubules assemble through the chromatin-dependent pathway or from acentriolar MTOCs (Dumont and Desai, 2012). In these acentrosomal oocytes, microtubules can be seen originating locally from the chromatin itself or from discrete organizing centers (Huchon et al., 1981; Gard, 1992; Dumont et al., 2007; Schuh and Ellenberg, 2007; Colombie et al., 2008). By

Development (2017) 144, 1674-1686 doi:10.1242/dev.147504

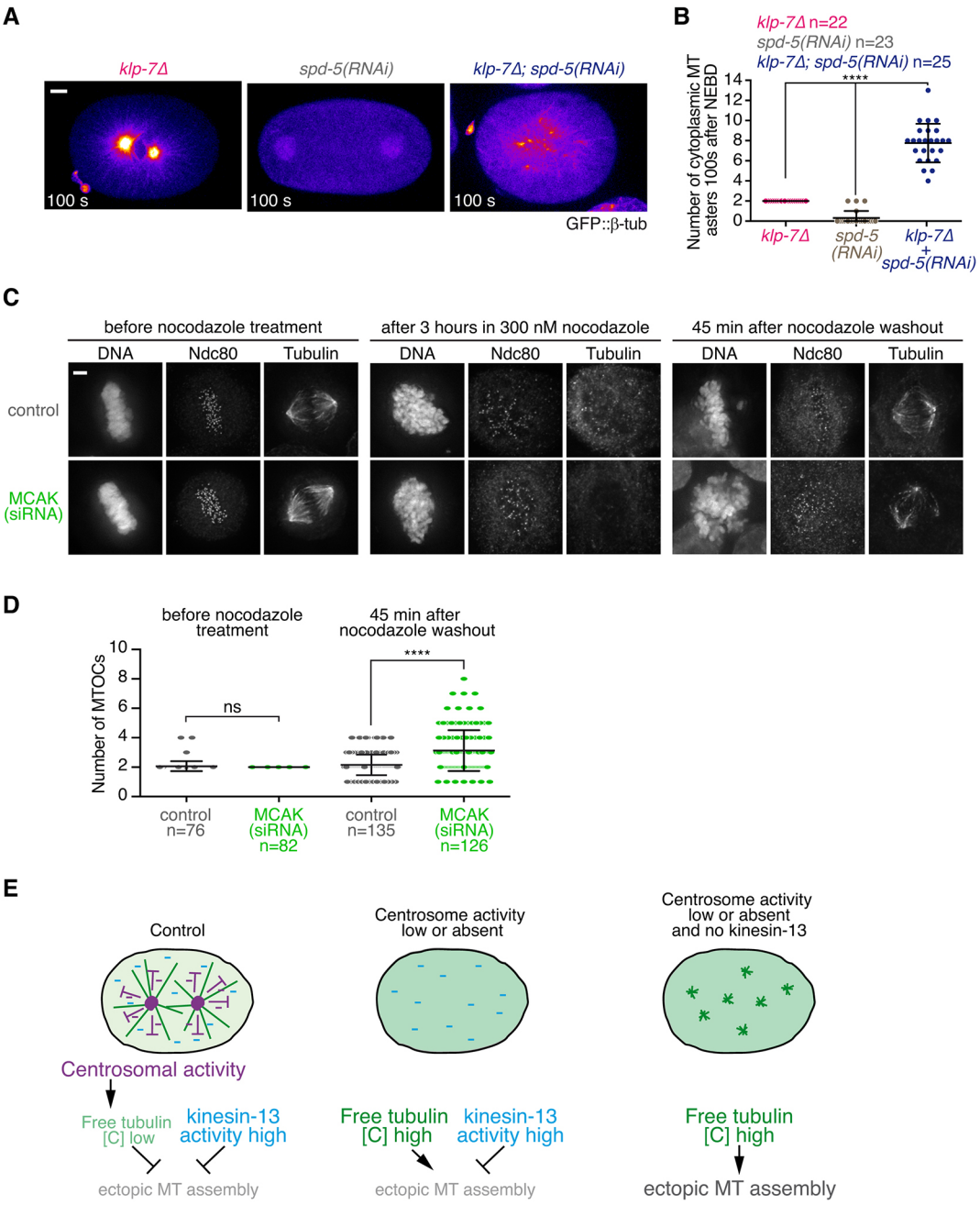

Fig. 6. Kinesin-13 depolymerases prevent ectopic microtubule assembly when centrosome function is low or absent. (A) Pseudocolored images from a live imaging experiment in GFP-tagged β-tubulin-expressing *klp-7Δ* or control zygotes 100 s after NEBD with or without *spd-5(RNAi)*. Multiple ectopic microtubule asters assemble in the absence of KLP-7 when centrosome activity is impaired after *spd-5(RNAi)*. Scale bar: 5 µm. (B) Quantification of the number of microtubule asters in *klp-7Δ* or control zygotes 100 s after NEBD with or without *spd-5(RNAi)*. Error bars represent s.d. Unpaired *t*-test with Welch's correction was used to determine significance (****P<0.0001). (C) Immunostaining of kinetochores (NDC80) and microtubules in control or MCAK-depleted HeLa cells before and after incubation for 3 h in 300 nM nocodazole or 45 min after nocodazole washout. Ectopic MTOCs are observed in MCAK-depleted cells only after nocodazole washout. Scale bar: 5 µm. (D) Quantification of the MTOC number in control or MCAK-depleted HeLa cells before nocodazole treatment. (P=0.0837) or 45 min after nocodazole washout (****P<0.0001). Unpaired *t*-test with Welch's correction was used to determine significance. Error bars represent s.d. (E) Model of kinesin-13-dependent ectopic microtubule assembly when centrosome activity is low or absent. In controls (right), the centrosomes incorporate most of the free tubulin and thus act as a microtubule polymerization-buffering system. The free tubulin concentration is low and does not allow spontaneous microtubule aster formation at a distance from the centrosomes. In the absence of centrosomes, the free tubulin concentration is high enough to allow spontaneous ectopic microtubule aster formation (left), unless kinesin-13 is active and destabilizes these ectopic asters (middle).

contrast, we found that in the *C. elegans* oocyte, microtubules, which are excluded from the nucleus before NEBD, assemble in the nuclear space after NEBD to form a diffuse cloud. This result is consistent with qualitative observations made in previous studies and with the lack of discrete MTOCs in this system (Yang et al., 2003). We found that spindle assembly is constrained within the space of the rupturing nuclear envelope. We thus propose that in *C. elegans* oocytes the space delimited by the nuclear envelope remnants acts as a diffuse MTOC. In KLP-7-depleted oocytes, NEBD occurred normally but the microtubule nuclear cloud did not

Development (2017) 144, 1674-1686 doi:10.1242/dev.147504

form and an excess of microtubules persisted around the breaking nuclear envelope throughout phase 1. This suggests that the function of KLP-7, which is cytoplasmic before and at NEBD, is to destabilize these perinuclear microtubules in order to release free tubulin necessary for the formation of the nuclear cloud.

Following formation of the microtubule nuclear cloud, bundling and cross-linking activities led to microtubule coalescence around meiotic chromosomes. This second step is likely to be under the control of microtubule motors previously implicated in successful meiotic divisions, such as dynein, the two redundant kinesin-14 family members KLP-15/16 (orthologs of NCD) and the kinesin-12 family member KLP-18 (ortholog of XKLP2 or KIF15) (Dernburg et al., 2000; Piano et al., 2000; Colaiacovo et al., 2002; Segbert et al., 2003; Wolff et al., 2016). We found that in the absence of a nuclear cloud of microtubules in KLP-7-depleted oocytes, the ectopic perinuclear microtubules are instead bundled and coalesce around chromosomes to form a seemingly normal multipolar spindle. However, the subsequent organization of microtubules into a bipolar spindle was impaired. Instead, abnormally dense multipolar spindles with long, disorganized and stable microtubules were formed.

Following bipolar spindle formation and chromosome alignment on a tight metaphase plate, drastic microtubule reorganization occurs that ultimately leads to chromosome segregation and PBE. We previously showed that chromosome segregation in the *C. elegans* oocyte is driven by an atypical kinetochore-independent mechanism (Dumont et al., 2010). In this system, central spindle organization is essential for chromosome segregation (Muscat et al., 2015; McNally et al., 2016). In agreement, we show here that KLP-7 depletion leads to disorganized central spindles that correlate with impaired chromosome segregation. Specifically, anaphase B, which normally accounts for most of the segregation process, does not occur. In line with this result, central spindle elongation was proposed to be specifically important for anaphase B chromosome movements (McNally et al., 2016). Live imaging of the minus-end marker GFP::ASPM-1 at this stage showed that microtubule minus-ends are distributed all over the disorganized central spindle instead of being concentrated toward chromosomes and generate an antiparallel microtubule overlap. We suspect that KLP-7 is required to generate this overlap by preventing excessive and/or ectopic microtubule elongation from chromosomes, where it is concentrated during meiotic anaphase (Fig. 1E) (Han et al., 2015). SPD-1 and the Centralspindlin complex (including CYK-4) have been shown to preferentially interact with overlapping microtubule plus-ends, which might explain their delocalization in the denser and disorganized central spindle that is assembled following *klp-7 (RNAi)* (Bieling et al., 2010; Davies et al., 2015).

In the absence of KLP-7, another striking defect in the organization of the microtubule network is the formation of multiple microtubule asters at the oocyte cortex. Although a cortical meshwork of microtubules is present in control oocytes, asters are normally not present at the cortex. A cytoplasmic pool of KLP-7 might be responsible for reducing the stability of this microtubule meshwork and to prevent ectopic aster formation. We observed that cortical asters located near the meiotic spindle often joined the spindles and contributed to the formation of the multipolar spindle. The minus-end-directed motor dynein, which is present throughout the cortex of the oocyte, is probably responsible for the aster aggregation that we observed (Crowder et al., 2015). Asters incorporated in the spindle could saturate the activity of microtubule motors and thus prevent normal spindle bipolarization.

Kinesin-13 depolymerases prevent ectopic microtubule assembly when centrosome function is low or absent

The ectopic asters observed in oocytes in the absence of KLP-7 disappeared abruptly at anaphase II and were never observed in mitotic embryos. During mitosis, KLP-7 depletion leads to increased astral microtubule density but does not lead to ectopic cortical aster formation (Srayko et al., 2005). We hypothesize that this difference is linked to the large size of the embryonic mitotic spindle as compared with the tiny oocyte spindles, and to the absence of functional centrosomes in oocytes, which are the dominant MTOCs during mitotic divisions (Hannak et al., 2002). Oocytes and the single-celled fertilized zygote share a common cytoplasmic composition, including the same concentration of tubulin heterodimers. The large astral spindle in zygotes contains a higher microtubule mass than the tiny meiotic spindles in oocytes. This leads to a lower cytoplasmic concentration of free tubulin heterodimer in zygotes compared with oocytes. The cytoplasmic tubulin concentration in oocytes is thus likely to be closer to the *in vivo* critical concentration at which microtubules can spontaneously nucleate and form microtubule asters. KLP-7 depolymerase activity must restrain this spontaneous microtubule assembly in oocytes. During mitosis, the centrosomes would thus act as a microtubule polymerization-buffering system and prevent overall spindle disorganization. By contrast, in oocytes depleted of KLP-7, free tubulin heterodimers are incorporated into all existing microtubule networks, including the perinuclear microtubules in unfertilized oocytes, and into the cortical meshwork and the spindle after fertilization, ultimately leading to its disorganization. Consistent with this interpretation we showed that, in the absence of KLP-7, microtubule asters spontaneously assembled during mitosis in the one-celled zygote only when the free tubulin heterodimer concentration was experimentally increased through reduction of centrosome activity. Similarly, in cultured human cells when centrosome activity was reduced (during microtubule regrowth after nocodazole washout), we observed a higher number of MTOCs after kinesin-13 MCAK depletion than in control cells. Similar ectopic asters have been observed in *Drosophila* oocytes depleted of the kinesin-13 KLP10A (Radford et al., 2012; Do et al., 2014). We propose that, when centrosome activity is reduced or absent, global microtubule destabilization by a kinesin-13 family member(s) is essential to prevent the formation of ectopic microtubule asters, which otherwise lead to spindle disorganization and chromosome mis-segregation (Fig. 6E). This previously uncharacterized function of kinesin-13 proteins defines a new level in the regulation of microtubule assembly *in vivo*, which is particularly important for the generation of euploid oocytes that lack centrosomes. As kinesin-13 motors are highly conserved across evolution, this new paradigm is likely to apply to other species and could further our understanding of human reproduction and the etiology of sterility.

MATERIALS AND METHODS

C. elegans strains and RNAi

C. elegans strains are listed in Table S2 and were maintained at 16°C or 23°C (Oegema et al., 2001). Primers for dsRNA production are listed in Table S3 (Oegema et al., 2001). L4 hermaphrodites were microinjected with dsRNA and incubated at 20°C for 48 h before processing.

HeLa cell culture and treatment

HeLa cells, tested monthly for mycoplasma contamination using a luminometer detection method (Lonza), were maintained in DMEM (Lonza) supplemented with 10% FBS and penicillin/streptomycin (Gibco) at 37°C in a humidified atmosphere with 5% CO_2. Cells were plated on glass coverslips coated with poly-L-lysine (Sigma-Aldrich). RNAi experiments

Development (2017) 144, 1674-1686 doi:10.1242/dev.147504

were conducted using RNAi MAX transfection reagent (Invitrogen) according to the manufacturer's guidelines. Previously published siRNA oligos were used to deplete MCAK (Domnitz et al., 2012). After 48 h of siRNA treatment, the cells were incubated for 2-3 h with 300 ng/ml nocodazole (Sigma, M1404). The nocodazole was then washed out five times with fresh DMEM and cells were left for 45 min in fresh DMEM. Cells were then briefly washed in PBS and fixed in PHEM (60 mM Pipes, 25 mM Hepes, 10 mM EGTA, 2 mM $MgCl_2$, pH 6.9) containing 4% formaldehyde for 10 min. Immunofluorescence was conducted using antibodies against mouse anti-α-tubulin (Sigma, T9026; used at 1 µg/ml) and human anti-NDC80 antibody (kind gift from Iain Cheeseman; used at 1 µg/ml). DNA was then counterstained with 1 µg/ml Hoechst.

Images were acquired on a DeltaVision Core deconvolution microscope (Applied Precision) equipped with a CoolSNAP HQ2 CCD camera (Photometrics). Twenty *z*-sections were acquired at 0.3 µm steps using a 100×1.4 NA Olympus U-PlanApo objective without binning. Maximal projections of stacks of interest after image deconvolution (SoftWorks) are presented. Equivalent exposure conditions were used between controls and drug-treated cells. Experiments were repeated three times. The number of spindle poles or the presence of ectopic microtubule foci in the cytoplasm was visually assessed and quantified.

Live imaging and metaphase I arrest

For *in utero* live imaging experiments, adult worms were anaesthetized using 100 mg tricaine (Sigma-Aldrich, E10521) and 10 mg tetramisol hydrochloride (Sigma-Aldrich, T1512) diluted in 1 ml M9 buffer. Immobilized worms were then mounted on a 2% agarose pad in M9 buffer between a slide and a coverslip. Live imaging was performed using a Nikon CFI APO LBDA S 40×/NA 1.25 water objective on a spinning disk confocal microscope (Roper Scientific) equipped with a CoolSNAP HQ2 camera, and acquisition parameters were controlled by MetaMorph 7 software (Molecular Devices). Four *z*-sections every 2 µm were acquired at 20 s intervals. Imaging on *ex utero* oocytes was performed as described (Dumont et al., 2010).

FRAP experiments were performed on *ex utero* oocytes using a Nikon CFI APO LBDA S 60×/NA 1.4 oil objective with 2×2 binning on a spinning disk confocal microscope equipped with the iLas Pulse FRAP/Photoactivation module (Roper Scientific). The extensive disassembly of microtubules observed during the spindle shrinkage phase could preclude measuring fluorescence recovery. To avoid this caveat and to measure fluorescence recovery in a steady state, we performed the FRAP experiments in the *mat-2(ax76ts)* temperature-sensitive (ts) strain that arrests in metaphase I when shifted to the restrictive temperature (26°C) (Golden et al., 2000). Stacks of four *z*-sections with a spacing of 2 µm were acquired every 3 s in the GFP channel before a single FRAP event of the entire surface of the metaphase spindle. After the FRAP event, images were acquired every 3 s for the first 120 s, then every 10 s for the following 100 s, and every 20 s for the last 500 s. A maximum projection of the four *z*-sections is presented for each time point. The average fluorescence was measured in a box around the metaphase spindle (Fspin) and in a box at a distance from the spindle in the cytoplasm (Fcyt). Normalization, correction and fitting of the measured fluorescence intensities were performed using Prism 6 software (GraphPad). Although we verified that the imaging conditions that we used did not lead to any significant photobleaching on embryos that did not undergo a FRAP event, the data were corrected (Fcor) for any potential photobleaching occurring during acquisition by multiplying each time point by Fcyt(0)/Fcyt(t). In order to be able to compare different experiments, the last prebleach and first postbleach time points were normalized to 1 and 0, respectively, by: FcorNormalized(t) = (Fcor(t)−FcorPost)/(FcorPre−FcorPost). The mean value of FcorNormalized was then calculated for individual embryos at each time point. The corresponding plot was fitted to a mono-exponential function and the half-time for recovery was extracted.

Image analysis and microtubule length calculation

Image analyses and quantifications were performed using Fiji (Schindelin et al., 2012) and Icy (de Chaumont et al., 2012) software. Kymographs were generated using the Multi Kymograph tool in Fiji.

For estimating the average length of microtubules at steady state, we used a simple mathematical model that links microtubule length distribution to dynamics parameters (Verde et al., 1992). In this model, L= (Rshrink×Rgrowth)/[(Rshrink×Fcat)−(Rgrowth×Fres)], where L is the average microtubule length, Rshrink and Rgrowth are the rates of microtubule shrinkage and growth, respectively, and Fcat and Fres are the frequencies of microtubule catastrophe and rescue, respectively.

Antibodies and immunofluorescence microscopy

Immunofluorescent staining was performed as described (Dumont et al., 2010). The rabbit anti-KLP-7 antibody was custom produced, validated in this study (see Fig. S1) and used at 1 µg/µl.

Graphs and statistical analysis

Experiments were repeated at least twice and a minimum number of ten oocytes were quantified for each experimental condition. All graphs were produced and statistical analyses performed with Excel (Microsoft) and Prism 6. Statistical significance was evaluated using unpaired *t*-tests with Welch's correction or one-way ANOVA.

Acknowledgements

We thank Jeremy Cramer from Cherry Biotech (Rennes, France) for allowing us to use pre-commercial development versions of the CherryTemp system; Patricia Moussounda for providing technical support; the Caenorhabditis Genetics Center (University of Minnesota, USA) for worm strains; the National BioResource Project (National Institute of Genetics, Japan) for the *tm2143* mutant strain; and Iain Cheeseman (Whitehead Institute for Biomedical Research, Cambridge, MA, USA) for the NDC80 bonsai antibody.

Competing interests

The authors declare no competing or financial interests.

Author contributions

Experiments were conceived by J.D. and were primarily performed and analyzed by E.G. and M.S. All strains used in this study were generated by M.S. and J.C.C. K.L., F.E., G.M. and B.L. performed some of the live imaging experiments and analyses. A.G.-K. and J.P.I.W. conceived, performed and analyzed the experiments in HeLa cells. J.C.C., J.P.I.W. and J.D. made the figures and wrote the manuscript.

Funding

E.G. is supported by an Association pour la Recherche sur le Cancer post-doctoral fellowship. This work was supported by Centre National de la Recherche Scientifique and Université Paris Diderot and by National Institutes of Health grants R01 GM117407 and DP2 OD008773 to J.C.C.; a Cancer Research UK Career Development Fellowship (C40377/A12840) to J.P.I.W.; and grants from the Agence Nationale de la Recherche (ANR-09-RPDOC-005-01), the Mairie de Paris (Programme Emergence) and the Fondation pour la Recherche Médicale (DEQ20160334869) to J.D. Deposited in PMC for release after 12 months.

Supplementary information

Supplementary information available online at
http://dev.biologists.org/lookup/doi/10.1242/dev.147504.supplemental

References

Alfaro-Aco, R. and Petry, S. (2015). Building the microtubule cytoskeleton piece by piece. *J. Biol. Chem.* **290**, 17154-17162.

Bieling, P., Telley, I. A. and Surrey, T. (2010). A minimal midzone protein module controls formation and length of antiparallel microtubule overlaps. *Cell* **142**, 420-432.

Cavazza, T., Malgaretti, P. and Vernos, I. (2016). The sequential activation of the mitotic microtubule assembly pathways favors bipolar spindle formation. *Mol. Biol. Cell* **27**, 2935-2945.

Cheeseman, I. M. (2014). The kinetochore. *Cold Spring Harb. Perspect. Biol.* **6**, a015826.

Colaiacovo, M. P., Stanfield, G. M., Reddy, K. C., Reinke, V., Kim, S. K. and Villeneuve, A. M. (2002). A targeted RNAi screen for genes involved in chromosome morphogenesis and nuclear organization in the Caenorhabditis elegans germline. *Genetics* **162**, 113-128.

Colombie, N., Cullen, C. F., Brittle, A. L., Jang, J. K., Earnshaw, W. C., Carmena, M., McKim, K. and Ohkura, H. (2008). Dual roles of Incenp crucial to the assembly of the acentrosomal metaphase spindle in female meiosis. *Development* **135**, 3239-3246.

Connolly, A. A., Sugioka, K., Chuang, C. H., Lowry, J. B. and Bowerman, B. (2015). KLP-7 acts through the Ndc80 complex to limit pole number in C. elegans oocyte meiotic spindle assembly. *J. Cell Biol.* **210**, 917-932.

Development (2017) 144, 1674-1686 doi:10.1242/dev.147504

Crowder, M. E., Flynn, J. R., McNally, K. P., Cortes, D. B., Price, K. L., Kuehnert, P. A., Panzica, M. T., Andaya, A., Leary, J. A. and McNally, F. J. (2015). Dynactin-dependent cortical dynein and spherical spindle shape correlate temporally with meiotic spindle rotation in Caenorhabditis elegans. *Mol. Biol. Cell* **26**, 3030-3046.

Davies, T., Kodera, N., Kaminski Schierle, G. S., Rees, E., Erdelyi, M., Kaminski, C. F., Ando, T. and Mishima, M. (2015). CYK4 promotes antiparallel microtubule bundling by optimizing MKLP1 neck conformation. *PLoS Biol.* **13**, e1002121.

de Chaumont, F., Dallongeville, S., Chenouard, N., Hervé, N., Pop, S., Provoost, T., Meas-Yedid, V., Pankajakshan, P., Lecomte, T., Le Montagner, Y. et al. (2012). Icy: an open bioimage informatics platform for extended reproducible research. *Nat. Methods* **9**, 690-696.

Dernburg, A. F., Zalevsky, J., Colaiacovo, M. P. and Villeneuve, A. M. (2000). Transgene-mediated cosuppression in the C. elegans germ line. *Genes Dev.* **14**, 1578-1583.

Desai, A., Verma, S., Mitchison, T. J. and Walczak, C. E. (1999). Kin I kinesins are microtubule-destabilizing enzymes. *Cell* **96**, 69-78.

Do, K. K., Hoang, K. L. and Endow, S. A. (2014). The kinesin-13 KLP10A motor regulates oocyte spindle length and affects EB1 binding without altering microtubule growth rates. *Biol. Open* **3**, 561-570.

Domnitz, S. B., Wagenbach, M., Decarreau, J. and Wordeman, L. (2012). MCAK activity at microtubule tips regulates spindle microtubule length to promote robust kinetochore attachment. *J. Cell Biol.* **197**, 231-237.

Dorn, J. F., Zhang, L., Paradis, V., Edoh-Bedi, D., Jusu, S., Maddox, P. S. and Maddox, A. S. (2010). Actomyosin tube formation in polar body cytokinesis requires Anillin in C. elegans. *Curr. Biol.* **20**, 2046-2051.

Dumont, J. and Brunet, S. (2010). Meiotic spindle assembly and chromosome segregation in oocytes. In *Oogenesis: The Universal Process* (ed. M.-H. Verlhac and A. Villeneuve), pp 269-290. Chichester, UK: John Wiley & Sons.

Dumont, J. and Desai, A. (2012). Acentrosomal spindle assembly and chromosome segregation during oocyte meiosis. *Trends Cell Biol.* **22**, 241-249.

Dumont, J., Petri, S., Pellegrin, F., Terret, M.-E., Bohnsack, M. T., Rassinier, P., Georget, V., Kalab, P., Gruss, O. J. and Verlhac, M.-H. (2007). A centriole- and RanGTP-independent spindle assembly pathway in meiosis I of vertebrate oocytes. *J. Cell Biol.* **176**, 295-305.

Dumont, J., Oegema, K. and Desai, A. (2010). A kinetochore-independent mechanism drives anaphase chromosome separation during acentrosomal meiosis. *Nat. Cell Biol.* **12**, 894-901.

Fabritius, A. S., Flynn, J. R. and McNally, F. J. (2011). Initial diameter of the polar body contractile ring is minimized by the centralspindlin complex. *Dev. Biol.* **359**, 137-148.

Gard, D. L. (1992). Microtubule organization during maturation of Xenopus oocytes: assembly and rotation of the meiotic spindles. *Dev. Biol.* **151**, 516-530.

Glotzer, M. (2005). The molecular requirements for cytokinesis. *Science* **307**, 1735-1739.

Golden, A., Sadler, P. L., Wallenfang, M. R., Schumacher, J. M., Hamill, D. R., Bates, G., Bowerman, B., Seydoux, G. and Shakes, D. C. (2000). Metaphase to anaphase (mat) transition-defective mutants in Caenorhabditis elegans. *J. Cell Biol.* **151**, 1469-1482.

Green, R. A., Paluch, E. and Oegema, K. (2012). Cytokinesis in animal cells. *Annu. Rev. Cell Dev. Biol.* **28**, 29-58.

Grill, S. W., Gönczy, P., Stelzer, E. H. K. and Hyman, A. A. (2001). Polarity controls forces governing asymmetric spindle positioning in the Caenorhabditis elegans embryo. *Nature* **409**, 630-633.

Hamill, D. R., Severson, A. F., Carter, J. C. and Bowerman, B. (2002). Centrosome maturation and mitotic spindle assembly in C. elegans require SPD-5, a protein with multiple coiled-coil domains. *Dev. Cell* **3**, 673-684.

Han, X., Adames, K., Sykes, E. M. E. and Srayko, M. (2015). The KLP-7 residue S546 is a putative aurora kinase site required for microtubule regulation at the centrosome in C. elegans. *PLoS ONE* **10**, e0132593.

Hannak, E., Oegema, K., Kirkham, M., Gönczy, P., Habermann, B. and Hyman, A. A. (2002). The kinetically dominant assembly pathway for centrosomal asters in Caenorhabditis elegans is gamma-tubulin dependent. *J. Cell Biol.* **157**, 591-602.

Heald, R. and Khodjakov, A. (2015). Thirty years of search and capture: The complex simplicity of mitotic spindle assembly. *J. Cell Biol.* **211**, 1103-1111.

Heald, R., Tournebize, R., Blank, T., Sandaltzopoulos, R., Becker, P., Hyman, A. and Karsenti, E. (1996). Self-organization of microtubules into bipolar spindles around artificial chromosomes in Xenopus egg extracts. *Nature* **382**, 420-425.

Huchon, D., Crozet, N., Cantenot, N. and Ozon, R. (1981). Germinal vesicle breakdown in the Xenopus laevis oocyte: description of a transient microtubular structure. *Reprod. Nutr. Dev.* **21**, 135-148.

Illingworth, C., Pirmadjid, N., Serhal, P., Howe, K. and FitzHarris, G. (2010). MCAK regulates chromosome alignment but is not necessary for preventing aneuploidy in mouse oocyte meiosis I. *Development* **137**, 2133-2138.

Kline-Smith, S. L., Khodjakov, A., Hergert, P. and Walczak, C. E. (2004). Depletion of centromeric MCAK leads to chromosome congression and segregation defects due to improper kinetochore attachments. *Mol. Biol. Cell* **15**, 1146-1159.

Lacroix, B., Bourdages, K. G., Dorn, J. F., Ihara, S., Sherwood, D. R., Maddox, P. S. and Maddox, A. S. (2014). In situ imaging in C. elegans reveals developmental regulation of microtubule dynamics. *Dev. Cell* **29**, 203-216.

Maddox, A. S., Azoury, J. and Dumont, J. (2012). Polar body cytokinesis. *Cytoskeleton* **69**, 855-868.

Maney, T., Hunter, A. W., Wagenbach, M. and Wordeman, L. (1998). Mitotic centromere-associated kinesin is important for anaphase chromosome segregation. *J. Cell Biol.* **142**, 787-801.

Maton, G., Edwards, F., Lacroix, B., Stefanutti, M., Laband, K., Lieury, T., Kim, T., Espeut, J., Canman, J. C. and Dumont, J. (2015). Kinetochore components are required for central spindle assembly. *Nat. Cell Biol.* **17**, 697-705.

McNally, K. P., Panzica, M. T., Kim, T., Cortes, D. B. and McNally, F. J. (2016). A novel chromosome segregation mechanism during female meiosis. *Mol. Biol. Cell* **27**, 2576-2589.

Mishima, M., Kaitna, S. and Glotzer, M. (2002). Central spindle assembly and cytokinesis require a kinesin-like protein/RhoGAP complex with microtubule bundling activity. *Dev. Cell* **2**, 41-54.

Muscat, C. C., Torre-Santiago, K. M., Tran, M. V., Powers, J. A. and Wignall, S. M. (2015). Kinetochore-independent chromosome segregation driven by lateral microtubule bundles. *Elife* **4**, e06462.

Nagaoka, S. I., Hassold, T. J. and Hunt, P. A. (2012). Human aneuploidy: mechanisms and new insights into an age-old problem. *Nat. Rev. Genet.* **13**, 493-504.

Oegema, K., Desai, A., Rybina, S., Kirkham, M. and Hyman, A. A. (2001). Functional analysis of kinetochore assembly in Caenorhabditis elegans. *J. Cell Biol.* **153**, 1209-1226.

Ohkura, H. (2015). Meiosis: an overview of key differences from mitosis. *Cold Spring Harb. Perspect. Biol.* **7**, pii: a015859.

Piano, F., Schetter, A. J., Mangone, M., Stein, L. and Kemphues, K. J. (2000). RNAi analysis of genes expressed in the ovary of Caenorhabditis elegans. *Curr. Biol.* **10**, 1619-1622.

Radford, S. J., Harrison, A. M. and McKim, K. S. (2012). Microtubule-depolymerizing kinesin KLP10A restricts the length of the acentrosomal meiotic spindle in Drosophila females. *Genetics* **192**, 431-440.

Rogers, G. C., Rogers, S. L., Schwimmer, T. A., Ems-McClung, S. C., Walczak, C. E., Vale, R. D., Scholey, J. M. and Sharp, D. J. (2004). Two mitotic kinesins cooperate to drive sister chromatid separation during anaphase. *Nature* **427**, 364-370.

Schindelin, J., Arganda-Carreras, I., Frise, E., Kaynig, V., Longair, M., Pietzsch, T., Preibisch, S., Rueden, C., Saalfeld, S., Schmid, B. et al. (2012). Fiji: an open-source platform for biological-image analysis. *Nat. Methods* **9**, 676-682.

Schuh, M. and Ellenberg, J. (2007). Self-organization of MTOCs replaces centrosome function during acentrosomal spindle assembly in live mouse oocytes. *Cell* **130**, 484-498.

Segbert, C., Barkus, R., Powers, J., Strome, S., Saxton, W. M. and Bossinger, O. (2003). KLP-18, a Klp2 kinesin, is required for assembly of acentrosomal meiotic spindles in Caenorhabditis elegans. *Mol. Biol. Cell* **14**, 4458-4469.

Srayko, M., Kaya, A., Stamford, J. and Hyman, A. A. (2005). Identification and characterization of factors required for microtubule growth and nucleation in the early C. elegans embryo. *Dev. Cell* **9**, 223-236.

Szollosi, D., Calarco, P. and Donahue, R. P. (1972). Absence of centrioles in the first and second meiotic spindles of mouse oocytes. *J. Cell Sci.* **11**, 521-541.

van der Voet, M., Berends, C. W. H., Perreault, A., Nguyen-Ngoc, T., Gönczy, P., Vidal, M., Boxem, M. and van den Heuvel, S. (2009). NuMA-related LIN-5, ASPM-1, calmodulin and dynein promote meiotic spindle rotation independently of cortical LIN-5/GPR/Galpha. *Nat. Cell Biol.* **11**, 269-277.

Verbrugghe, K. J. C. and White, J. G. (2004). SPD-1 is required for the formation of the spindle midzone but is not essential for the completion of cytokinesis in C. elegans embryos. *Curr. Biol.* **14**, 1755-1760.

Verde, F., Dogterom, M., Stelzer, E., Karsenti, E. and Leibler, S. (1992). Control of microtubule dynamics and length by cyclin A-dependent and cyclin B- dependent kinases in Xenopus egg extracts. *J. Cell Biol.* **118**, 1097-1108.

Walczak, C. E. and Heald, R. (2008). Mechanisms of mitotic spindle assembly and function. *Int. Rev. Cytol.* **265**, 111-158.

Walczak, C. E., Mitchison, T. J. and Desai, A. (1996). XKCM1: a Xenopus kinesin-related protein that regulates microtubule dynamics during mitotic spindle assembly. *Cell* **84**, 37-47.

Walczak, C. E., Gayek, S. and Ohi, R. (2013). Microtubule-depolymerizing kinesins. *Annu. Rev. Cell Dev. Biol.* **29**, 417-441.

Wolff, I. D., Tran, M. V., Mullen, T. J., Villeneuve, A. M. and Wignall, S. M. (2016). Assembly of Caenorhabditis elegans acentrosomal spindles occurs without evident microtubule-organizing centers and requires microtubule sorting by KLP-18/kinesin-12 and MESP-1. *Mol. Biol. Cell* **27**, 3122-3131.

Wordeman, L. and Mitchison, T. J. (1995). Identification and partial characterization of mitotic centromere- associated kinesin, a kinesin-related protein that associates with centromeres during mitosis. *J. Cell Biol.* **128**, 95-104.

Yang, H.-Y., McNally, K. and McNally, F. J. (2003). MEI-1/katanin is required for translocation of the meiosis I spindle to the oocyte cortex in C. elegans. *Dev. Biol.* **260**, 245-259.

Development (2017) 144, 1674-1686 doi:10.1242/dev.147504

Zhang, X., Ma, C., Miller, A. L., Katbi, H. A., Bement, W. M. and Liu, X. J. (2008). Polar body emission requires a RhoA contractile ring and Cdc42-mediated membrane protrusion. *Dev. Cell* **15**, 386-400.

Zou, J., Hallen, M. A., Yankel, C. D. and Endow, S. A. (2008). A microtubule-destabilizing kinesin motor regulates spindle length and anchoring in oocytes. *J. Cell Biol.* **180**, 459-466.

FIGURE S1

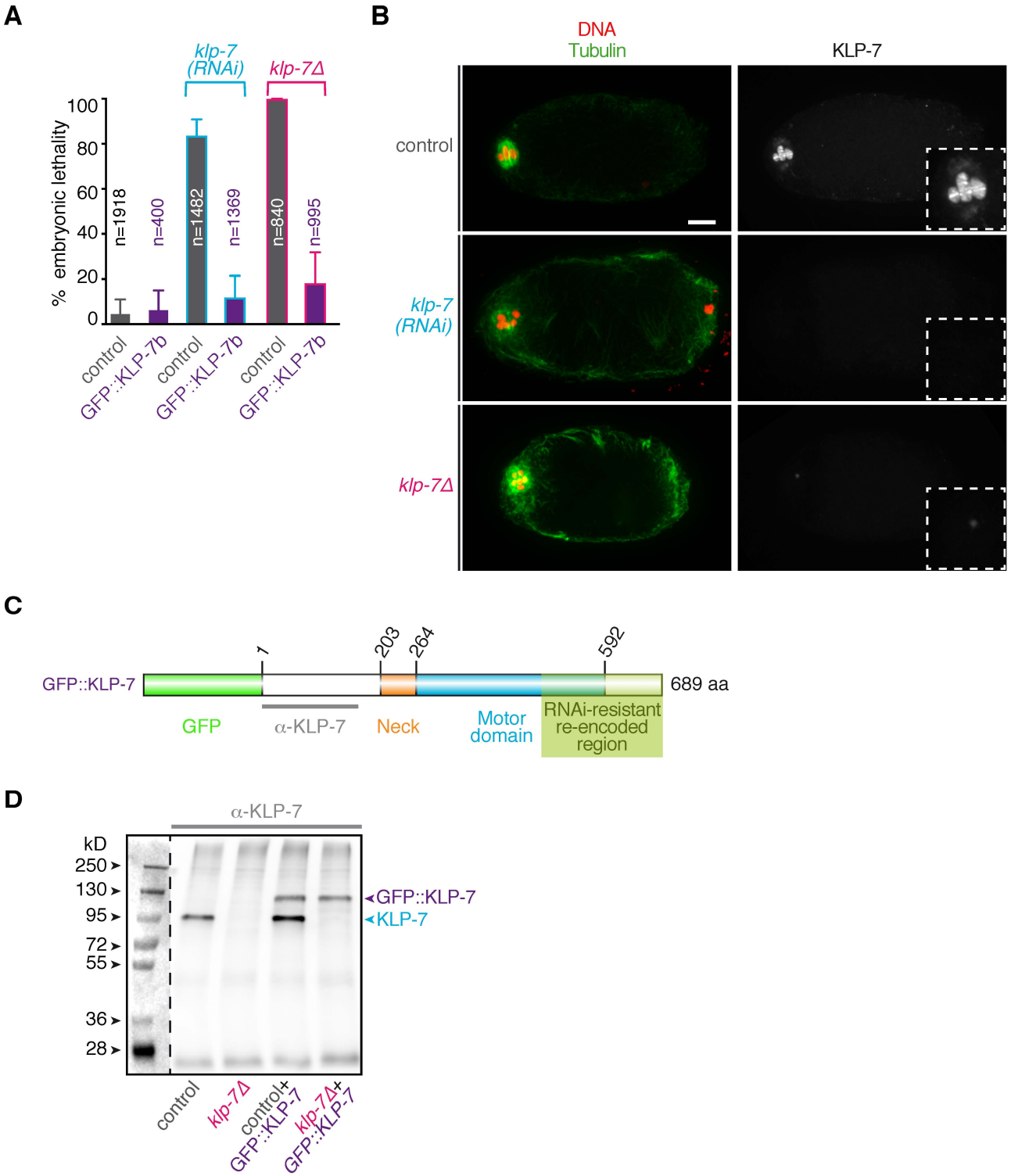

Figure S1. Efficiency and specificity of the RNAi-mediated depletion of KLP-7. (A) Quantification of the embryonic lethality associated with *klp-7(RNAi)* or in the *klp-7* deletion (*klp-7Δ*) in presence or absence of RNAi-resistant GFP::KLP-7. Error bars represent the s.d. (B) Immunostainings of KLP-7 during metaphase I in control, *klp-7(RNAi)* and *klp-7Δ* oocytes (Right). A close-up of the spindle region is shown in the white dashed box. Microtubules (green) and chromosomes (red) are also stained (Left). Scale bar, 5 µm. (C) Schematic representation of the RNAi-resistant GFP::KLP-7 transgene displaying the functional domains, the re-encoded RNAi-resistant region and the region recognized by the anti-KLP-7 antibody used in this study. (D) Western blot on whole worm extracts with the indicated genotypes. The rabbit KLP-7 antibody recognized both endogenous and GFP-tagged KLP-7 proteins.

FIGURE S2

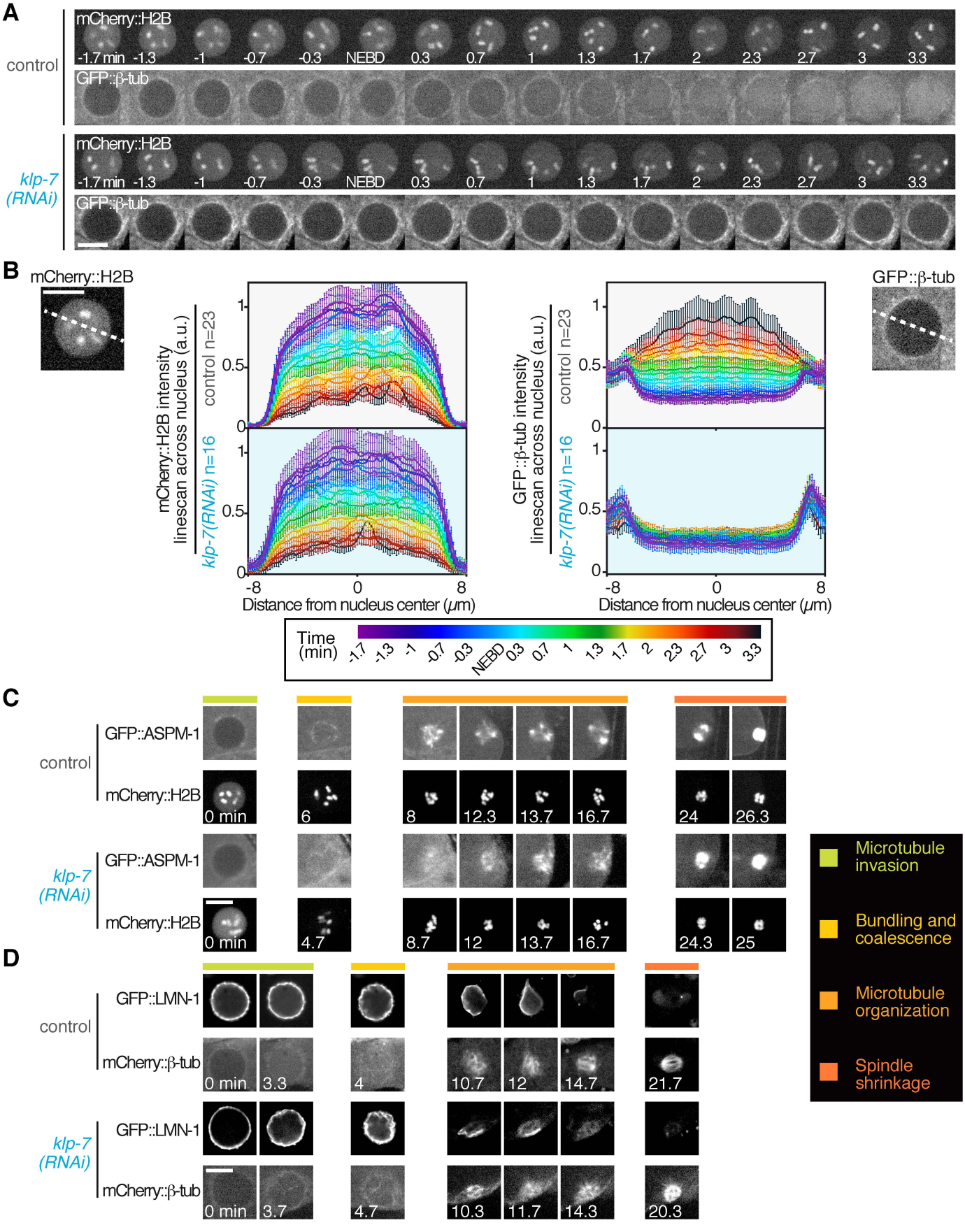
A
control
mCherry::H2B
-1.7 min -1.3 -1 -0.7 -0.3 NEBD 0.3 0.7 1 1.3 1.7 2 2.3 2.7 3 3.3
GFP::β-tub
klp-7 (RNAi)
mCherry::H2B
-1.7 min -1.3 -1 -0.7 -0.3 NEBD 0.3 0.7 1 1.3 1.7 2 2.3 2.7 3 3.3
GFP::β-tub
B
mCherry::H2B
mCherry::H2B intensity linescan across nucleus (a.u.)
control n=23
klp-7(RNAi) n=16
Distance from nucleus center (μm)
GFP::β-tub
GFP::β-tub intensity linescan across nucleus (a.u.)
control n=23
klp-7(RNAi) n=16
Distance from nucleus center (μm)
Time (min)
-1.7 -1.3 -1 -0.7 -0.3 NEBD 0.3 0.7 1 1.3 1.7 2 2.3 2.7 3 3.3
C
control
GFP::ASPM-1
mCherry::H2B
0 min 6 8 12.3 13.7 16.7 24 26.3
klp-7 (RNAi)
GFP::ASPM-1
mCherry::H2B
0 min 4.7 8.7 12 13.7 16.7 24.3 25
Microtubule invasion
Bundling and coalescence
Microtubule organization
Spindle shrinkage
D
control
GFP::LMN-1
mCherry::β-tub
0 min 3.3 4 10.7 12 14.7 21.7
klp-7 (RNAi)
GFP::LMN-1
mCherry::β-tub
0 min 3.7 4.7 10.3 11.7 14.3 20.3

Figure S2. KLP-7 function during meiotic spindle assembly.

(A) Still images from *in vivo* live imaging in GFP-tagged β-tubulin and mCherry-tagged H2B-expressing oocytes showing the first phase of meiosis I spindle assembly in the indicated conditions. Timings are relative to NEBD. (B) Fluorescence intensity linescan of mCherry-tagged H2B and GFP-tagged β-tubulin across the nucleus between 1.7 min before NEBD and 3.3 min after NEBD (timings are color-coded according to the horizontal scale presented at the bottom). 0 μm corresponds to the center of the nucleus. The sample size (number of oocytes analyzed) is provided in the figure and was generated by aggregation over 6 independent experiments. Error bars represent the s.e.m. (C) Still images from in vivo live imaging in GFP-tagged ASPM-1 and mCherry-tagged H2B-expressing oocytes showing the 4 phases (indicated by the color-coded line above each image) of meiosis I spindle assembly in the indicated conditions. Timings are relative to NEBD. (D) Still images from *in vivo* live imaging in GFP-tagged LMN-1 and mCherry-tagged H2B-expressing oocytes showing the 4 phases (indicated by the color-coded line above each image) of meiosis I spindle assembly in the indicated conditions. Timings are relative to NEBD. Scale bars, 10 μm.

FIGURE S3

A

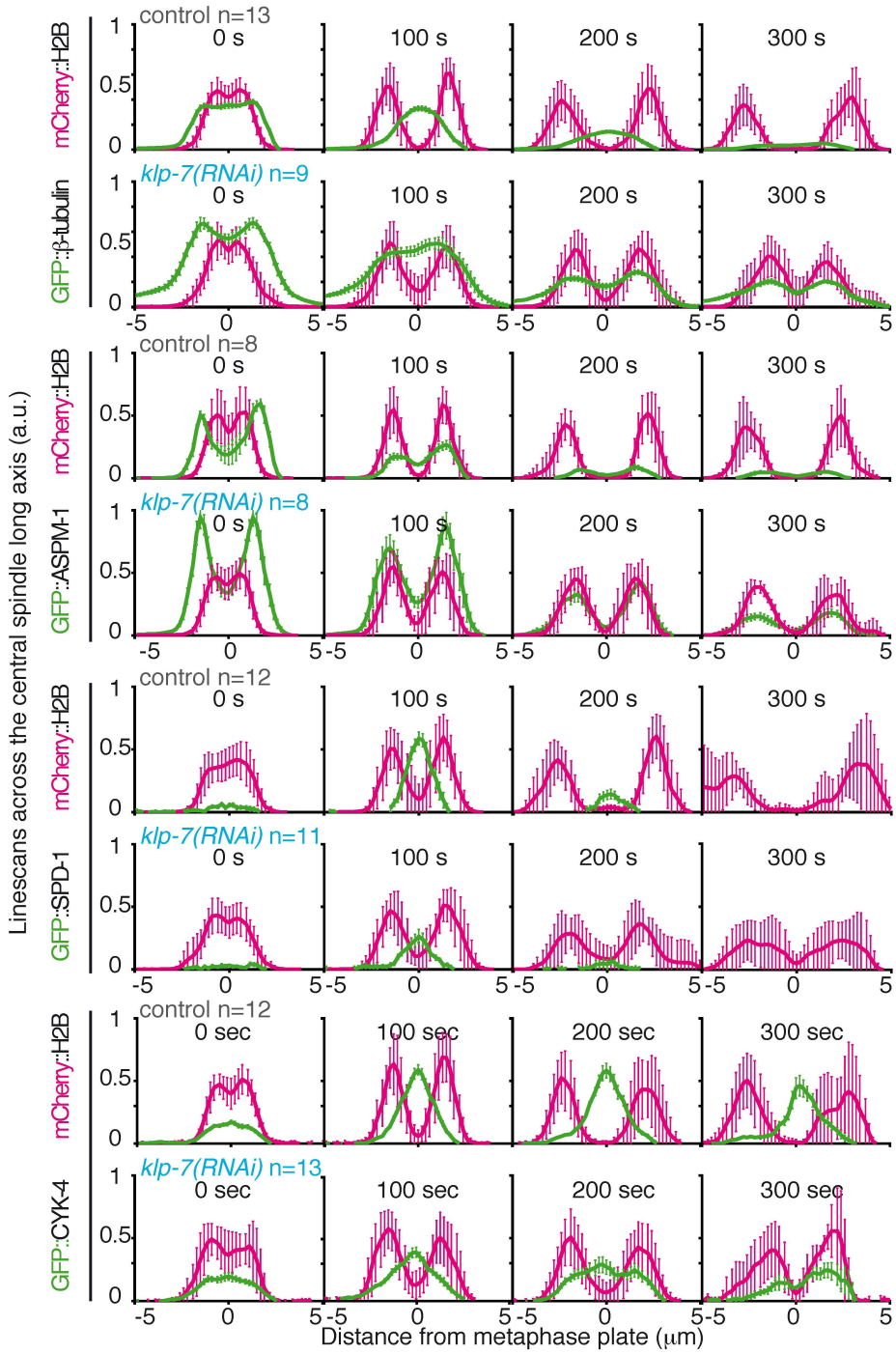

Figure S3. KLP-7 is essential for central spindle assembly.

(A) Fluorescence intensity linescan of mCherry-tagged H2B and the indicated GFP-tagged protein across the central spindle long axis during anaphase I. 0 μm corresponds to the position of chromosomes in metaphase (metaphase plate). The sample size (number of oocytes analyzed) is provided in the figure and was generated by aggregation over 3 independent experiments. Error bars represent the s.d.

FIGURE S4

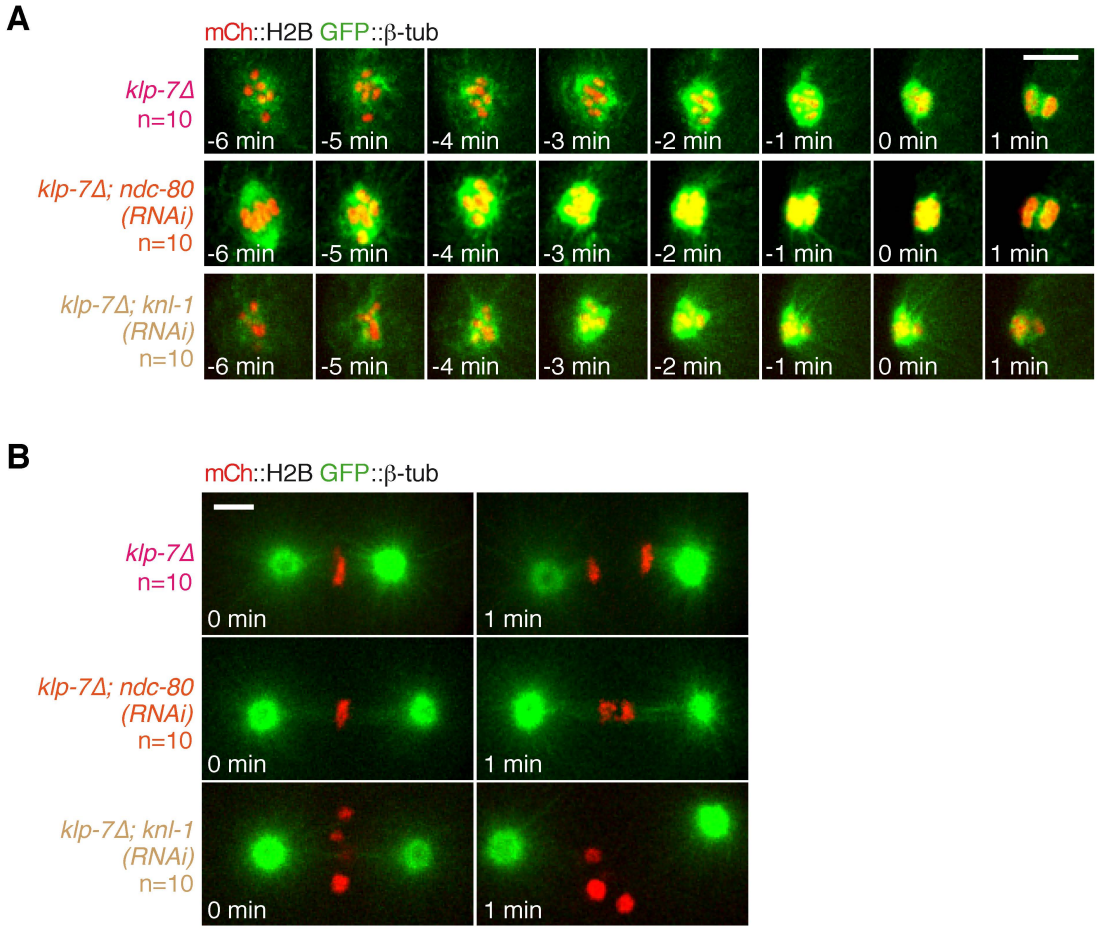

Figure S4. Kinetochore component depletion does not stably rescue spindle bipolarity in the absence of KLP-7 .

(A) Still images from live imaging in GFP-tagged β-tubulin and mCherry-tagged H2B-expressing oocytes in the indicated conditions between prometaphase I and anaphase I. Timings are relative to anaphase I onset. Scale bar, 5 μm. (B). Still images from live imaging in GFP-tagged β-tubulin and mCherry-tagged H2B-expressing zygotes in the indicated conditions. The same embryos were followed from metaphase of meiosis I to completion of the first mitosis. KLP-7 -deleted zygotes have excessive astral pulling forces leading to central spindle rupture and abnormally fast sister chromatid segregation; NDC-80-depleted zygotes do not align chromosomes properly and display chromosomal bridges during anaphase; KNL-1-depleted embryos exhibit a "kinetochore null" phenotype characterized by clustering of chromosomes from each pronucleus, absence of a metaphase plate, and no chromosome segregation. Timings are relative to anaphase onset. Scale bar, 5 μm.

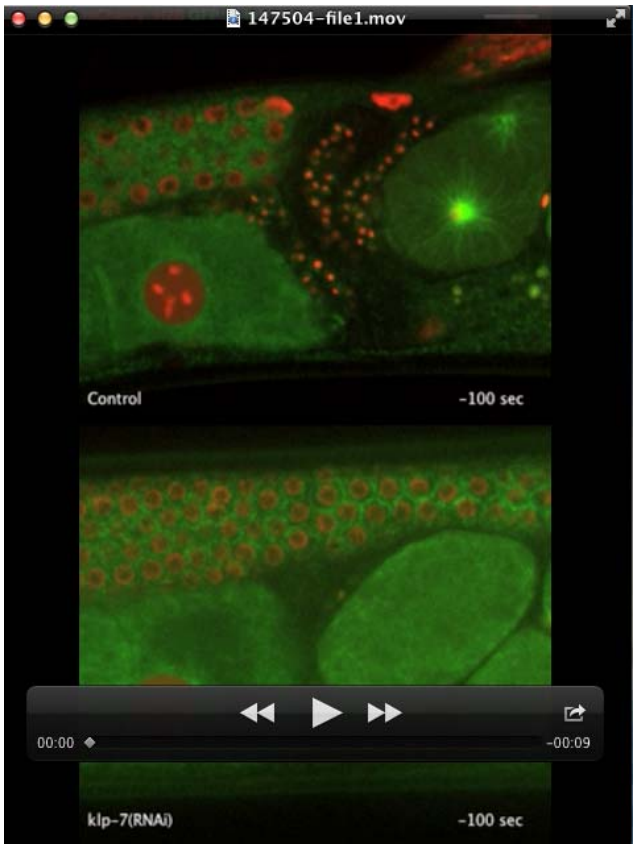

Movie 1. *In utero* live imaging of immobilized worms expressing GFP-tagged β-tubulin and mCherry-tagged H2B. Scale bar, 10 μm.

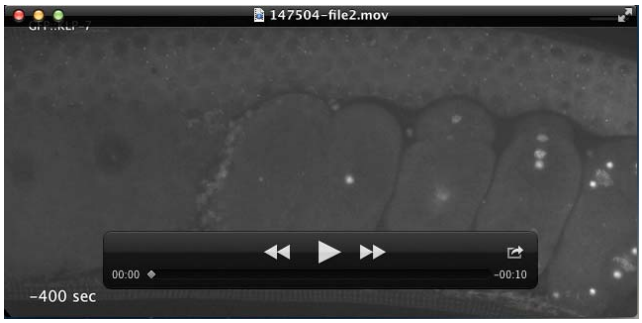

Movie 2. *In utero* live imaging of an immobilized worm expressing GFP-tagged KLP-7. Scale bar, 10 μm.

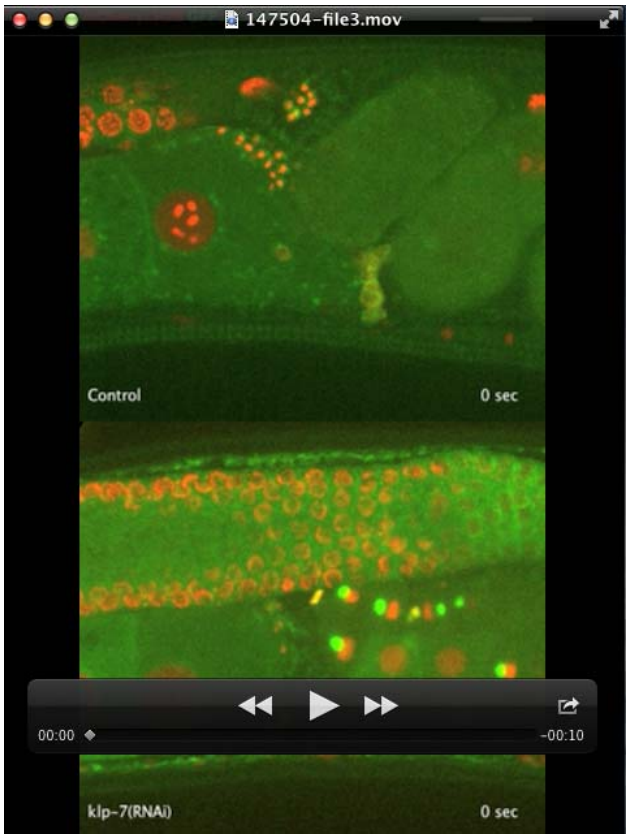

Movie 3. *In utero* live imaging of immobilized worms expressing GFP-tagged ASPM-1 and mCherry-tagged H2B. Scale bar, 10 μm.

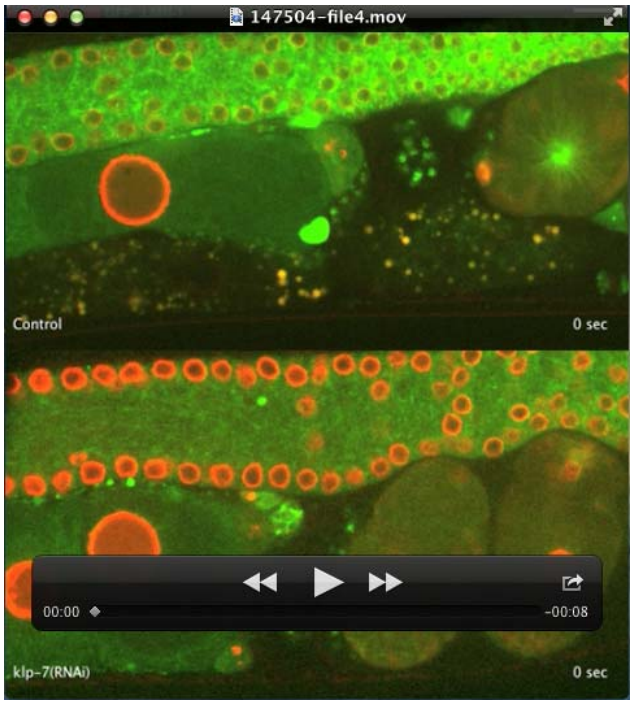

Movie 4. *In utero* live imaging of immobilized worms expressing GFP-tagged LMN-1 and mCherry-tagged β-tubulin. Scale bar, 10 μm.

Movie 5. Live imaging of fertilized oocytes expressing GFP-tagged β-tubulin and mCherry-tagged H2B. Scale bar, 10 μm.

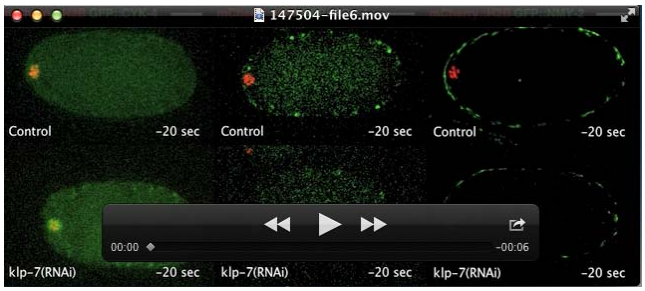

Movie 6. Live imaging of oocytes expressing GFP-tagged CYK-4 (Left), GFP-tagged SPD-1 (Middle) or GFP-tagged NMY-2 (Right), and mCherry-tagged H2B. Scale bar, 10 μm.

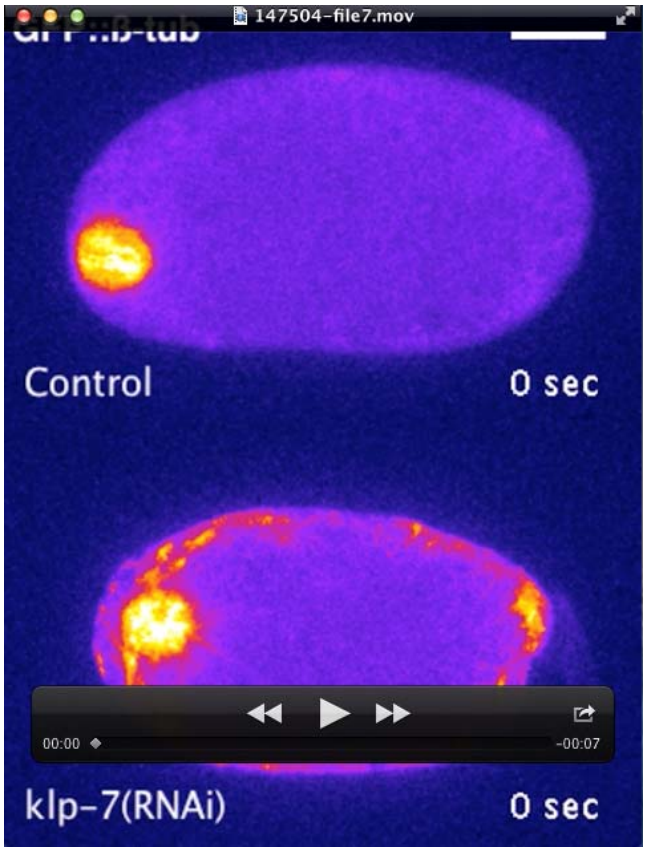

Movie 7. FRAP experiment in fertilized oocytes expressing GFP-tagged β-tubulin. Scale bar, 10 μm.

SUPPLEMENTAL TABLE S1 – *p values for Figure 3*

Chromosomes	Control vs *klp-7(RNAi)*			
	0 s	**100 s**	**200 s**	**300 s**
β-tub	p=0.0002	p<0.0001	p<0.0001	p<0.0001
ASPM-1	p=0.0009	p<0.0001	p<0.0001	p<0.0001
CYK-4	p=0.6608	p=0.5646	p=0.0010	p=0.0023
SPD-1	p=0.5971	p=0.0675	p=0.0028	p=0.0094

Central Spindle	Control vs *klp-7(RNAi)*			
	0 s	**100 s**	**200 s**	**300 s**
β-tub	p<0.0001	p=0.0021	p=0.1251	p=0.0197
ASPM-1	p<0.0001	p=0.0016	p=0.4725	p=0.3638
CYK-4	p=0.3475	p=0.0015	p=0.011	p=0.0426
SPD-1	p=0.3004	p=0.0024	p=0.7895	p=0.3464

	Control vs *klp-7(RNAi)*				
	0 s	**100 s**	**200 s**	**300 s**	**400s**
NMY-2	p=0.0241	p=0.0010	p=0.0005	p=0.0086	p=0.2718

SUPPLEMENTAL TABLE S2 – *C. elegans* strains used in this study

*[*unc-119(ed3)?*] was present in the parental strains, but these strains have not been directly sequenced to determine if the *unc-119* gene contains the *ed3* mutation.

Strain	Genotype
N2	*Wild Type (Ancestral N2 Bristol)*
JCC483	*ojIs1[Ppie-1::GFP::tbb-2::3'tbb-2]; unc-119(ed3)III?; ltIs37[pAA64; Ppie-1::mCherry::his-58; unc-119 (+)]IV**
JDU320	*klp-7(tm2143); ijmSi41[pJD457; Pmex-5::GFP::klp-7b reencoded::3'tbb-2; cb-unc-119(+)]I; ijmSi41[pJD456; Pmex-5::mCherry::tbb-2::3'tbb-2]II; unc-119(ed3) III?**
JDU106	*ijmSi7 [pJD348; Pmex-5::GFP::tbb-2::3'tbb-2; mCherry::his-11::3'tbb-2; cb-unc-119(+)]I; mat-2(ax76)II; unc-119(ed3)III?**
JDU316	*klp-7(tm2143); ojIs1[Ppie-1::GFP::tbb-2::3'tbb-2]; unc-119(ed3) III?; ltIs37[pAA64; Ppie-1/mCherry::his-58; unc-119 (+)] IV**
JDU115	*ijmSi11 [pJD359; Pmex-5::spd-1::sfGFP::3'spd-1; cb-unc-119(+)]II; unc-119(ed3)III?; ijmSi25 [pJD425; Pmex-5::TagRFP::zen-4::3'tbb-2; cb-unc-119(+)]III; ltIs37 [pAA64; Ppie-1::mCherry::his-58; unc-119 (+)]IV**
JDU384	*unc-119(ed3) III?; ltIs37 [pAA64; Ppie-1::mCherry::his-58; unc-119 (+)] IV; zuIs45[Pnmy-2::nmy-2::GFP::3'nmy-2; unc-119(+)] V**
JDU385	*unc-119(ed3) III?; ltIs37 [pAA64; Ppie-1::mCherry::his-58; unc-119 (+)] IV; ltIs16[pASM07; Ppie-1::GFP::cyk-4::3'tbb-2; unc-119 (+)]**
JDU293	*ijmSi65 [pJD528; Pmex-5::sfGFP::aspm-1::3'tbb-2; cb-unc-119(+)] II; unc-119(ed3) III?; ltIs37 [pAA64; Ppie-1::mCherry::his-58; unc-119 (+)] IV**
JDU184	*unc-119(ed3) III?; ijmSi49 [pJD479; Pmex-5::GFP::lmn-1::3'tbb-2]I ; ijmSi41 [pJD456 _Pmex-5::mCherry::tbb2::3'tbb-2]II**
JDU180	*ijmSi40 [pJD457; Pmex-5::GFP::klp-7b reencoded::3'tbb-2; cb-unc-119(+)]I; ijmSi31 [pJD446 _Pmex-5_mCherry::his11::3'tbb-2]II; unc-119(ed3) III?**

SUPPLEMENTAL TABLE S3

Primers d templates used for dsRNA production

*Lowercase letters denote T3 and T7 sequences included for RNA synthesis

Gene	Primer 1*	Primer 2*	Template	Final [C]
K11D9.1 *(klp-7)*	5' aattaaccctcactaaagg TGATCTGGAATATGGCGTGA 3'	5' taatacgactcactatagg GTGCTTCTGCCAACAAACG 3'	N2 cDNA	1
K11D9.1 *(klp-7)*	5' aattaaccctcactaaagg CCATGCTAATGTCTTCACACG 3'	5' taatacgactcactatagg CCGCTGAAATGGATACGAGT 3'	N2 cDNA	1.3
W01B6.9 *(ndc-80)*	5' aattaaccctcactaaagg GATGACAAGTACATTCAGAGATTATA CAAATGATC 3'	5' taatacgactcactatagg GTGGTTCAAGATTCATTTGAATATTAA GTCCACTG 3'	N2 cDNA	2.6
C02F5.1 *(knl-1)*	5' aattaaccctcactaaagg AATCTCGAATCACCGAAATGTC 3'	5' taatacgactcactatagg TTCACAAACTTGGAAGCCGCTG 3'	N2 gDNA	1.5
F56A3.4 *(spd-5)*	5' aattaaccctcactaaagg TGTCGCAACCAGTTCTGAAT 3'	5' taatacgactcactatagg ATGGAGGCAAATTGTTGCTG 3'	N2 gDNA	1.1